



FINITE-DIFFERENCE COMPATIBLE ENTROPY-CONSERVING SCHEMES FOR THE COMPRESSIBLE EULER EQUATIONS*

A PREPRINT

 **Carlo De Michele**
 Fluid Mechanics Unit
 Italian Aerospace Research Center (CIRA)
 Capua (CE), Italy
 c.demichelle@cira.it

 **Ayaboe K. Edoh**
 Amentum — Edwards Air Force Base
 CA 93524, USA
 ayaboe.edoh.ctr@us.af.mil

 **Gennaro Coppola**
 Dipartimento di Ingegneria Industriale
 Università di Napoli “Federico II”
 Napoli, Italy
 gcoppola@unina.it

November 26, 2024

ABSTRACT

This paper introduces a family of entropy-conserving finite-difference discretizations for the compressible flow equations. In addition to conserving the primary quantities of mass, momentum, and total energy, the methods also preserve kinetic energy and pressure equilibrium. The schemes are based on finite-difference (FD) representations of the logarithmic mean, establishing and leveraging a broader link between linear and nonlinear two-point averages and FD forms. The schemes are locally conservative due to the summation-by-parts property and therefore admit a local flux form, making them applicable also in finite-volume and finite-element settings. The effectiveness of these schemes is validated through various test cases (1D Sod shock tube, 1D density wave, 2D isentropic vortex, 3D Taylor Green vortex) that demonstrate exact conservation of entropy along with conservation of the primary quantities and preservation of pressure equilibrium.

Keywords compressible flow · finite difference · entropy conservation · summation-by-parts · logarithmic mean · kinetic-energy-preserving · pressure-equilibrium-preserving

1 Introduction

It is generally considered advantageous to discretize the compressible flow equations using supra-conservative [1] schemes that are not only able to conserve the primary invariants, but also additional secondary ones. Aside from the conservation of mass, momentum and total energy, structure-preserving methods for flows typically seek to improve discrete consistency with other properties such as entropy, kinetic energy, pressure-equilibrium, angular momentum, helicity, enstrophy, etc. [2, 3, 4, 5, 6]. In addition to improving the physical relevance and accuracy of the solution field, incorporating more consistencies can improve numerical stability, the benefits of which have been witnessed in increasingly complex physical settings such as for thermally-perfect, multi-component, and reacting gases [7, 8, 9]. For example, kinetic energy serves as a bounded L_2 estimate on the velocity variables for incompressible flows, while enstrophy serves a similar role with respect to a vorticity variable treatment [10, 11]. Such specialized quantities thus constitute mathematical entropies, which allow for a more rigorous statement on the robustness of the solution—even in the absence of natural stabilization mechanisms such as diffusion. Developing these structure-preserving methods

*Distribution Statement A: Approved for Public Release; Distribution is Unlimited. AFRL-2024-6076.

is therefore attractive for achieving a robust yet minimally-dissipative method for use when calculating flows that would otherwise be sensitive to numerical damping, such as in Large Eddy Simulations of high-Reynolds number configurations [12].

For compressible flows, kinetic energy no longer provides a bounded estimate on the flow field. Instead, the thermodynamic entropy (s) is often used, as its conservation yields an energy-like statement with respect to a set of special transformation variables (i.e., the entropy variables)²; this notion is furthermore strongly tied to the symmetrization of the Euler equations [14]. To this end, the current work introduces a new class of entropy-conserving methods for the compressible Euler system. Notably, these schemes have the additional property of being compatible with finite differencing.

Entropy-conserving (EC) methods have traditionally been designed in terms of two-point numerical fluxes that are based on a jump condition constraint introduced by Tadmor [15]. Their extension to high-order is then achieved via the notion of flux differencing [16, 17], wherein various low-order two-point fluxes are assembled in a type of Richardson extrapolation. This overall flux framework naturally lends itself to the finite volume (FV) community and has also gained wide use for achieving entropy consistency with modern finite element (FE) schemes [18, 19]. The congruence between flux (i.e., weak) forms and derivative (i.e., strong) forms is generally understood when discretizing linear functions with finite difference (FD) methods [20, 21]. A link between strong and weak forms, however, can also be established for nonlinearly stable discretizations in special instances. For example, the entropy-conservative treatment of Burgers equation can be expressed in a conservative FD form via a quadratic skew-symmetric splitting of the nonlinear term that induces the Heronian mean [22, 23]. While discretely equivalent, the respective methods entail different algorithmic overheads in terms of their implementation, particularly when extending to high-order. Such a direct duality between finite differencing and EC flux forms also exists for the incompressible flow equations [11]; however, the link has not yet been established in the context of the compressible Euler equations and may facilitate the discovery of new schemes.

Although FD formulations for the Euler equations can be designed to preserve linear invariants in addition to other properties like being kinetic-energy-preserving (KEP) and pressure-equilibrium-preserving (PEP), they traditionally do not exhibit the *strict* EC property. However, a notable class of FD splittings with heightened EC capabilities have been identified, which may be characterized as being *quasi* entropy-conserving methods (qEC). These include, among others, the recently developed kinetic-energy-entropy-preserving (KEEP) methods [3, 24]. The qEC schemes admit efficient FD representations and have been shown to greatly enhance numerical robustness across compressible regimes despite only being approximately entropy conserving. Interesting to note, is that the flux form associated with these FD-qEC methods emulates the flux form's structure of Ranocha's EC scheme [25, 26]³; the main point of contrast, however, is how the density (ρ) and internal energy (e) variables are averaged at the flux interface for the convective flux. A variety of other qEC methods that feature this same structure have recently been proposed [28] and termed asymptotically entropy-conserving; however, these forms are inherently flux-based in nature and are not traditionally associated with a finite difference splitting approach. While FD-qEC methods induce their flux averages (arithmetic or geometric) on the density and internal energy variables via quadratic and cubic splittings of the convective terms [29, 30], this framework does not readily admit the logarithmic-type means that are necessary for recovering strict conservation of the thermodynamic entropy in the case of perfect gases. However, in the same way that standard FD discretizations (with central schemes) of the divergence and advective forms of the convective terms have been linked to numerical fluxes based on bilinear and trilinear interpolations [21, 28], it is of interest to find FD discretizations linked to a Tadmor-type EC method such as Ranocha's flux.

The current work develops new finite-difference compatible methods that are strictly EC in the context of a single-component ideal gas with the calorically-perfect assumption. In order to achieve this, the intended nonlinear logarithmic flux averages for density and internal energy, $\tilde{\rho}$ and \tilde{e} , are first shown to be expressible as quotients of differences and then are explicitly introduced as auxiliary variables in the FD discretization of the compressible Euler system. Rather than satisfying a Tadmor jump condition on the fluxes, the new methods are derived by requiring point-wise cancellation of the spurious volumetric terms that are induced in the discrete entropy equation that is associated with the primary system. Enforcing these cancellations naturally reveals the necessary form of the special auxiliary variables; it also highlights the inherent relation between the choice in FD stencils and the derivative-based representation of the logarithmic means. While it is possible to make FD methods *globally* entropy conserving via correction procedures [21, 31], the current framework goes beyond by avoiding source terms in the resulting discrete entropy equation. In

²A precise energy statement is available when considering conservation for the class of Harten entropies $h(s)$ [13]. However, unlike the thermodynamic entropy, these functions do not admit provable stability for Navier-Stokes configurations that include Fourier conduction terms.

³Ranocha's flux is equivalent to the earlier EC scheme of Chandrashekar [27] in terms of the convective treatment; however, the two methods differ in how the pressure terms are calculated, with Ranocha's rendition enabling pressure-equilibrium-preservation and also having a direct finite difference representation.

addition to being EC, the new methods are made to be KEP and PEP as well. Throughout, we employ finite differencing based on diagonal-norm summation-by-parts (SBP) operators [32, 33], including biased renditions [34, 35, 36]. Notably, viable biased EC methods are identified for the first time—a feat that is facilitated by the current FD perspective. A finite difference form of Ranocha’s EC flux is then shown to be recovered as a special symmetric weighting of the two-point forward and backward biased operators.

The paper is organized as follows: Section 2 provides preliminaries in terms of the governing equations and the SBP-based finite difference stencils; Section 3 presents derivative-based representations of specialized nonlinear means; Section 4 introduces the new FD-EC methods; Section 5 confirms the intended scheme properties relative to various test cases (1D density wave, 1D Sod shock tube, 2D isentropic vortex, 3D Taylor-Green vortex); and finally Section 6 provides summary remarks and suggestions for further research.

2 Preliminaries

To better specify the context of our analysis, we start by considering the compressible Euler equations in d -dimensions, written as the balance equations for mass, momentum and total energy for a single-component gas in the absence of viscous and thermal effects

$$\frac{\partial \rho}{\partial t} = -\frac{\partial \rho u_n}{\partial x_n} = -\mathcal{C}_\rho \quad (1)$$

$$\frac{\partial \rho u_m}{\partial t} = -\left(\frac{\partial \rho u_n u_m}{\partial x_n} + \frac{\partial p}{\partial x_m}\right) = -(\mathcal{C}_{\rho u_m} + \mathcal{P}_{\rho u_m}) \quad (2)$$

$$\frac{\partial \rho E}{\partial t} = -\left(\frac{\partial \rho u_n E}{\partial x_n} + \frac{\partial p u_n}{\partial x_n}\right) = -(\mathcal{C}_{\rho E} + \mathcal{P}_{\rho E}) \quad (3)$$

where m and n are integers ranging between 1 and d (the dimension) with repeated index notation being presumed. In Eqs. (1)–(3), ρ is the density, u_m is the Cartesian velocity in direction m , p is the pressure, and E is the total energy per unit mass which is made up of the sum of internal and kinetic energies ($E = e + \frac{1}{2} \sum_{m=1}^d u_m^2$). The equations are furthermore categorized in terms of the convective and pressure operators, \mathcal{C} and \mathcal{P} respectively. Kinetic energy consistency (i.e., that the combination mass and momentum induce a viable kinetic energy representation) and energy consistency (i.e., that the total energy is composed of the internal energy representation as well as the induced kinetic energy form) [21, 3] are motivated by the following additional analytic relations

$$\begin{aligned} \mathcal{P}_{\rho E} &= \sum_{m=1}^d u_m \mathcal{P}_{\rho u_m} + \mathcal{P}_{\rho e} \\ &= \sum_{m=1}^d \left(u_m \frac{\partial p}{\partial x_m} + p \frac{\partial u_m}{\partial x_m} \right) \end{aligned} \quad (4)$$

$$\begin{aligned} \mathcal{C}_{\rho E} &= \mathcal{C}_{\rho k} + \mathcal{C}_{\rho e} \quad \text{with } \mathcal{C}_{\rho k} = \sum_{m=1}^d \left[u_m \mathcal{C}_{\rho u_m} - \frac{1}{2} u_m^2 \mathcal{C}_\rho \right] \\ &= \frac{\partial \rho u_n k}{\partial x_n} + \frac{\partial \rho u_n e}{\partial x_n} \quad \text{with } k = \frac{1}{2} \sum_{m=1}^d u_m^2 \end{aligned} \quad (5)$$

Based on the additional physical constraints implied by the above, one is then left to determine the discrete representations of the following: \mathcal{C}_ρ , $\mathcal{C}_{\rho u_m}$, $\mathcal{C}_{\rho e}$, $\mathcal{P}_{\rho u_m}$, and $\mathcal{P}_{\rho e}$.

2.1 Entropy analysis

We assume that pressure and internal energy are linked by the ideal gas equation of state, which implies $p = (\gamma - 1)\rho e$, that the specific heats at constant pressure and volume and their ratio $\gamma = c_p/c_v$ are constant, and that $e = c_v T$ where T is the absolute temperature. In this context, the thermodynamic entropy per unit mass is via Gibbs relation as

$$ds = c_v \frac{dp}{p} - c_v \gamma \frac{d\rho}{\rho} \rightarrow s = c_v \cdot \log(p/\rho^\gamma) = c_v \cdot \log e - c_v(\gamma - 1) \cdot \log \rho, \quad (6)$$

which presumes normalized quantities. The entropy can then be shown to satisfy the conservation equation

$$\frac{\partial \rho s}{\partial t} = -\frac{\partial \rho u_n s}{\partial x_n}. \quad (7)$$

Eq. (7), which is valid in general for an arbitrary equation of state, is a statement that for non-viscous adiabatic flows the entropy of material particles remains unchanged, which in turn implies that global entropy within an Eulerian volume Ω does not change in time, except due to inflow or outflow at the boundaries. Eq. (7) is a consequence of the system of Euler equations (1)–(3) and of basic thermodynamics, and does not constitute an independent balance principle⁴. As such, smooth solution fields satisfying Eqs. (1)–(3) also satisfy Eq. (7). To see this, consider the set of $(2 + d)$ entropy variables

$$w \triangleq \frac{\partial \rho s}{\partial [\rho, \rho u_m, \rho E]} = \frac{1}{T} \cdot \left[sT - e - \frac{p}{\rho} + \frac{1}{2} \sum_{m=1}^d u_m^2, -u_m, 1 \right] = \underbrace{[w_\rho, w_{\rho u_m}, w_{\rho E}]}_{[w_1, \dots, w_{2+d}]} \quad (8)$$

and their contraction with the governing system:

$$\begin{aligned} \frac{\partial \rho s}{\partial t} &= \sum_{m=1}^{2+d} w_m \cdot \frac{\partial q_m}{\partial t} = w_\rho \cdot \frac{\partial \rho}{\partial t} + w_{\rho u_m} \cdot \frac{\partial \rho u_m}{\partial t} + w_{\rho E} \cdot \frac{\partial \rho E}{\partial t} \\ &= \frac{1}{T} \left(sT - e - \frac{p}{\rho} \right) \cdot \frac{\partial \rho}{\partial t} + \frac{1}{T} \cdot \frac{\partial \rho e}{\partial t} \\ &= s \cdot \frac{\partial \rho}{\partial t} + \rho \cdot \underbrace{\left(\frac{1}{T} \cdot \frac{\partial e}{\partial t} - \frac{p}{\rho^2 T} \cdot \frac{\partial \rho}{\partial t} \right)}_{\partial s / \partial t} \end{aligned} \quad (9)$$

The above manipulations invoke two key relations: 1) energy consistency (i.e., $\partial \rho e = \partial \rho E - (\sum_{m=1}^d u_m \partial \rho u_m - \frac{1}{2} u_m^2 \partial \rho) = \partial(\rho E - \frac{1}{2} \sum_{m=1}^d \rho u_m^2)$) and 2) Gibbs relation (i.e., $T \partial s = \partial e - (p/\rho^2) \partial \rho$). When turning to discrete approximations, however, these types of links are typically lost in the sense that a consistent discretization of the system (1)–(3) does not imply that the discrete entropy is globally conserved. This behavior can be traced back to the failure of nominal operators to satisfy the usual rules of calculus that are valid for continuous operators—namely the product, chain, and summation-by-parts rules. EC schemes are designed, however, to exactly reproduce these structural properties of the continuous set of equations at the discrete level.

We will focus on the spatial discretization of the system of Eqs. (1)–(3) in the context of a semidiscretized procedure. This means that the analysis will assume that temporal integration can be carried out at the continuous level, whereas spatial approximation is obtained by using a discrete method. The framework of a conservative Finite Difference (FD) method is adopted, where variables constitute the nodal values of the continuous unknown functions over a (typically uniform) Cartesian mesh. The formulation used is *conservative* in the sense that convective and derivative terms are approximated by numerical schemes that can be expressed as sum of differences of numerical fluxes at adjacent nodes along each Cartesian direction. This property discretely reproduces the divergence structure of the convective terms in Eqs. (1)–(7) and is hence referred to as the discretization's *local conservation* property. *Global conservation* (i.e., the property that the total amount of the balanced quantity is not affected by the convective terms, except for boundary contribution) is then guaranteed by the telescoping property, mimicking what happens at the continuous level.

For the sake of simplicity, but without loss of generality, we will expose our theory when possible with reference to the one-dimensional version of the system (1)–(3), such that $(m, n) = 1$. The discretization of the space coordinate x is made by considering a uniform mesh with nodal coordinates x_i and width (Δx) . Although not described herein, the extension to non-uniform meshes can be accomplished by taking into account the variable sizes of the discretization into the time-derivative terms ([37]), such as via the grid metrics Jacobian for curvilinear grids [33].

2.2 Conservative finite difference stencils

In what follows, some difference operators will be used, and they are here defined. First, consider a general finite difference stencil evaluated at node i

$$(\partial_x \phi)_i \approx (\delta \phi)_i = \frac{1}{\Delta x} \sum_k d_{i,i+k} \cdot \phi_{i+k} \quad (10)$$

In the above, we note that the FD stencil coefficients $d_{i,i+k}$ are dependent on the node at which the derivative is being estimated. Herein, we assume that the progression of stencils is arranged such as to satisfy a Summation-by-Parts (SBP)

⁴Note that analogous conservation statements can be written for special functions of the entropy, $h(s)$, as proposed by Harten [13]. However, we focus on the thermodynamic entropy herein.

property [33, 32], which is a discrete form of integration-by-parts, $\int_{\Omega} u dv = (-\int_{\Omega} v du + (uv)|_{\partial\Omega})$. Considering a general quadratic decomposition of the input $\phi = uv$, then the SBP property for stencils δ^c associated with a centered operator is expressed as

$$\sum_i h_i \cdot u_i(\delta^c v)_i = -\sum_i h_i \cdot v_i(\delta^c u)_i + (u_r v_r - u_\ell v_\ell) \quad (11)$$

where $(\cdot)_{\ell/r}$ correspond to consistent approximations of the function at the left and right boundaries. Note that on the interior of the domain, away from boundaries, the δ^c stencils above are central and asymmetric. In the case of classic finite difference SBP operators featuring nodes at the boundary, then $(\cdot)_{\ell/r}$ is the nodal value at the boundary itself such that $u_\ell v_\ell = (uv)_\ell$; however, additional interpretations are possible via the generalized SBP formalism [32] which accommodates the interpretation of such values as being consistent extrapolations or quasi-interpolations of the near boundary data. The above SBP statement can be further extended to biased dual-pair SBP operators with local difference stencils δ^\pm [38, 34, 36] as

$$\sum_i h_i \cdot u_i(\delta^\pm v)_i = -\sum_i h_i \cdot v_i(\delta^\mp u)_i + (u_r v_r - u_\ell v_\ell) \quad (12)$$

with the relationship that

$$\delta^c = (\delta^+ + \delta^-)/2 \quad (13)$$

and where $(\delta^+ - \delta^-)$ recovers an artificial dissipation term. In the above, h_i are scaling factors associated with a diagonal-norm of the SBP operator and can be interpreted as a quadrature rule [39]. Rearranging terms in Eqs. (11) and (12) reveals the quadratically-split ‘‘advection form’’ (i.e., $u\delta v + v\delta u$) that has been shown to yield a conservative telescoping like representation [20, 40, 37]. The nominal ‘‘divergence form’’ (e.g., $\delta(uv)$) also features a conservative telescoping property. In either case, general finite-volume fluxes can be derived from the SBP-compatible finite difference stencils via a recursive relation

$$\mathcal{F}_{i+1/2} = \begin{cases} h_i \cdot \delta^\pm(uv) + \mathcal{F}_{i-1/2} & \text{such that } \mathcal{F}_{1/2} \equiv \mathcal{F}_\ell = (uv)_\ell \\ h_i \cdot (u_i(\delta^\pm v)_i + v_i(\delta^\mp u)_i) + \mathcal{F}_{i-1/2} & \text{such that } \mathcal{F}_{1/2} \equiv \mathcal{F}_\ell = u_\ell v_\ell \end{cases} \quad (14)$$

where $\mathcal{F}_{i+1/2}$ are interface fluxes induced by the SBP discretization that live on a dual grid, $\bar{x}_{i+1/2}$, whose spacing is tied to the norm scaling such that $h_i = (\bar{x}_{i+1/2} - \bar{x}_{i-1/2})$ with $x_{1/2} \equiv x_\ell$ [41]. In effect, global conservation along with an identifiable flux (anywhere in the domain, such as the boundary) is sufficient for guaranteeing a telescoping flux property throughout [37]. While written in terms of the biased operators, Eq. (14) also applies to the central operators per Eq. (13).

The stencil coefficients $d_{i,i+k}$ in Eq. (10) and their progression in space may be conveyed in the form of matrices D acting on a vector of nodal solution data. For example, the standard second-order (two-point) finite difference SBP central operator and its dual decomposition are the following (assuming $(\Delta x) = 1$ for convenience),

(two-point stencils) : (15)

$$\underbrace{\begin{bmatrix} -1 & 1 & & & & & \\ -1/2 & 0 & 1/2 & & & & \\ & & \dots & & & & \\ & & -1/2 & 0 & 1/2 & & \\ & & & -1 & 1 & & \end{bmatrix}}_{D^c = \frac{1}{2}(D^+ + D^-)} = \frac{1}{2} \cdot \begin{bmatrix} -2 & 2 & & & & & \\ & -1 & 1 & & & & \\ & & \dots & & & & \\ & & & -1 & 1 & & \\ & & & 0 & 0 & & \end{bmatrix} + \frac{1}{2} \cdot \begin{bmatrix} 0 & 0 & & & & & \\ -1 & 1 & & & & & \\ & & \dots & & & & \\ & & -1 & 1 & & & \\ & & & -2 & 2 & & \end{bmatrix} \quad (16)$$

where the associated diagonal norm scaling is $H = \text{diag}([\frac{1}{2}, 1, \dots, 1, \frac{1}{2}])$ [35]. Note that the red and black rows in Eq. (16) represent the boundary versus interior stencils, respectively⁵. For this two-point operator, one can derive simple two-point fluxes responsible for calculating the interior interface fluxes $\mathcal{F}_{i+1/2}$ from the nodal data. For the interior central stencil we have

$$\begin{aligned} \delta_{2\text{pt}}(uv) &\longrightarrow \mathcal{F}(u, v)_{i+1/2, \text{div}} = \frac{(uv)_{i+1} + (uv)_i}{2} \triangleq \overline{uv} \\ u\delta_{2\text{pt}}v + v\delta_{2\text{pt}}u &\longrightarrow \mathcal{F}(u, v)_{i+1/2, \text{adv}} = \frac{u_{i+1}v_i + u_i v_{i+1}}{2} \triangleq \overline{\overline{uv}} \end{aligned} \quad (17)$$

⁵The central operator in (16) is second order on the interior and first order on the boundary. Meanwhile the biased operators feature a reduction in order, being first order on the interior and zeroth order (i.e., inconsistent) at the boundaries.

and for the interior biased stencils we have

$$\begin{aligned}
\delta_{2\text{pt}}^+(uv) &\longrightarrow \mathcal{F}^+(u, v)_{i,\text{div}} = (uv)_{i+1} \\
\delta_{2\text{pt}}^-(uv) &\longrightarrow \mathcal{F}^-(u, v)_{i,\text{div}} = (uv)_i \\
u\delta_{2\text{pt}}^+v + v\delta_{2\text{pt}}^-u &\longrightarrow \mathcal{F}^+(u, v)_{i,\text{adv}} = u_iv_{i+1} = \mathcal{F}^-(v, u)_{i,\text{adv}}
\end{aligned} \tag{18}$$

It is important to note that the interior advective form's flux for the two-point central operator is symmetric in its arguments; however, this is not the case for the biased splitting, which would provide additional flexibility in tailoring the behavior of the discretizations—for example with respect to interacting with sharp gradients in the solution field etc. In special cases (e.g., interior nodes discretized by central stencils) such two-point fluxes can be combined to express the fluxes associated with high-order operators [20, 41] in the fashion of Richardson type extrapolations. A convex combination of the divergence and advective forms is then possible and known to produce an independent averaging of the inputs. For example, when these forms are evenly weighted, we have

$$\begin{aligned}
\frac{1}{2} [\delta_{2\text{pt}}(uv) + u\delta_{2\text{pt}}v + v\delta_{2\text{pt}}u] &\longrightarrow \frac{1}{2} [\mathcal{F}(u, v)_{\text{div}} + \mathcal{F}(u, v)_{\text{adv}}]_{i+1/2} = \frac{u_{i+1}+u_i}{2} \frac{v_{i+1}+v_i}{2} \\
\frac{1}{2} [\delta_{2\text{pt}}^+(uv) + u\delta_{2\text{pt}}^+v + v\delta_{2\text{pt}}^-u] &\longrightarrow \frac{1}{2} [\mathcal{F}^+(u, v)_{\text{div}} + \mathcal{F}^+(u, v)_{\text{adv}}]_{i+1/2} = \frac{u_{i+1}+u_i}{2} v_{i+1} \\
\frac{1}{2} [\delta_{2\text{pt}}^-(uv) + u\delta_{2\text{pt}}^-v + v\delta_{2\text{pt}}^+u] &\longrightarrow \frac{1}{2} [\mathcal{F}^-(u, v)_{\text{div}} + \mathcal{F}^-(u, v)_{\text{adv}}]_{i+1/2} = \frac{u_{i+1}+u_i}{2} v_i \\
\frac{1}{2} [\delta_{2\text{pt}}^+(uv) + u\delta_{2\text{pt}}^-v + v\delta_{2\text{pt}}^+u] &\longrightarrow \frac{1}{2} [\mathcal{F}^+(u, v)_{\text{div}} + \mathcal{F}^-(u, v)_{\text{adv}}]_{i+1/2} = u_{i+1} \frac{v_i+v_{i+1}}{2} \\
\frac{1}{2} [\delta_{2\text{pt}}^-(uv) + u\delta_{2\text{pt}}^+v + v\delta_{2\text{pt}}^-u] &\longrightarrow \frac{1}{2} [\mathcal{F}^-(u, v)_{\text{div}} + \mathcal{F}^+(u, v)_{\text{adv}}]_{i+1/2} = u_i \frac{v_i+v_{i+1}}{2}
\end{aligned} \tag{19}$$

Further combinations are also possible upon considering combinations of the central and biased schemes (not shown). Such even weighting of the divergence and advective forms has been shown to be beneficial in terms of reducing nonlinear aliasing errors, at least in the context of central stencils [29, 42, 43, 44].

3 Specialized means via finite differences

In the previous section, a correspondence has been mentioned between finite difference discretizations of derivatives of products of two variables and numerical fluxes in the case of two-point discretizations. In particular, the divergence and advective forms with such central or unsymmetric difference operators have been associated with the class of two-point fluxes based on arithmetic averages. In special instances, finite difference splitting can also be used to induce a two-point geometric average [45, 6]—for example, this happens when considering $\phi = (\phi^{1/2} \phi^{1/2})$, in which case $\mathcal{F}(\phi^{1/2}, \phi^{1/2})_{i+1/2,\text{adv}} = \mathcal{F}^\pm(\phi^{1/2}, \phi^{1/2})_{i+1/2,\text{adv}} = \sqrt{\phi_i \phi_{i+1}}$. However, in many applications, more general fluxes comprised of nonlinear averages are necessary. These fluxes would seem to be outside the possible schemes that can be generated by classical finite difference discretizations, which are based on linear derivative formulas. For example, with respect to designing EC schemes, one needs access to other nonlinear averages such as logarithmic means. Yet it is has not been evident how to induce such expressions from a splitting technique. It seems then natural to inquire if there is a generalized approach within the finite difference framework to obtaining the discrete equations coming from schemes based on nonlinear flux functions.

By considering the fluxes associated with the general split forms for central or biased derivative operators in Eqs. (17)–(19), one observes that the application of the product rule in manipulating the convective term leads to various formulations which, although equivalent on a continuous ground, are associated with different fluxes with various interpolations that are all based on arithmetic averages for the product of two variables. However, the product rule is a special case of the *chain* rule, which is also not satisfied by discrete operators, and is associated with the composition of arbitrary nonlinear functions other than the simple product of two variables. From this observation, it is argued that to obtain fluxes in which a nonlinear average arises, of the type of the logarithmic mean appearing in the Ranocha's EC mass flux [25] ($\mathcal{F}_\rho = \bar{\rho}^{(\log)} \bar{u}$ where $\bar{\rho}^{(\log)} = (\rho_{i+1} - \rho_i) / (\log \rho_{i+1} - \log \rho_i)$), nonlinear transformations based on the chain rule have to be used to express the variables and/or their products. These transformations give different expressions that are equivalent on a continuous ground but furnish different approximations when discretely treated. In these discrete forms, the peculiarities of the nonlinear transformation are expected to emerge by determining the form of the fluxes through new nonlinear averages.

The case of the logarithmic mean is exemplary and is easily treated by using the transformation

$$\rho = \left(\frac{1}{\rho}\right)^{-1} = \left(\frac{d \log \rho}{d \rho}\right)^{-1} = \frac{d \rho}{d \log \rho} \quad (20)$$

where the last equality holds by virtue of the inverse function theorem applied to the bijective function $\log \rho$. In Eq. (20) the nonlinear transformation expressing ρ is specified through a derivative to make the chain rule relevant. By using Eq. (20) in the evaluation of the convective term for the continuity equation, one has

$$\frac{\partial \rho u}{\partial x} = \frac{\partial}{\partial x} \left(\frac{d \rho}{d \log \rho} u \right). \quad (21)$$

Although the equality in Eq. (21) is exact on a continuous ground, the discretization of the right-hand side will be associated with numerical fluxes that are different than those associated with the classical divergence form of the left-hand side. Moreover, using split forms and various choices for the approximations of the derivative of ρ furnishes different expressions for the fluxes, as for the split forms described in Eqs. (17)–(19). This type of procedure, in which FV schemes based on nonlinear fluxes are formulated as FD approximations, can be useful because a generalized treatment of the FD formulations can generate new potentially useful discretizations. An example is studied in Section 4 with reference to EC formulations based on the logarithmic mean.

A generalization of this procedure can be attempted by using a class of transformations associated with more general nonlinear averages, among which logarithmic and arithmetic means are particular cases. A sufficiently general transformation based on the use of derivatives to express a variable ϕ is given by the following relation, valid for positive values of ϕ :

$$\phi = \frac{\beta}{\beta + 1} \frac{d \phi^{\beta+1}}{d \phi^{\beta}}. \quad (22)$$

The validity of Eq. (22) is easily verified by observing that the function ϕ^{β} is a strictly monotone function for positive values of ϕ . This implies that the relation $\phi^{\beta} = g(\phi)$ can be inverted to give $\phi = g^{-1}(\phi^{\beta})$. For this last point, the inverse function theorem gives

$$\frac{d g^{-1}}{d \phi^{\beta}} = \frac{1}{d g / d \phi} \quad (23)$$

from which one can manipulate Eq. (22) to give

$$\begin{aligned} f_{\bar{\phi}}(\beta) &\triangleq \frac{\beta}{\beta + 1} \frac{d \phi^{\beta+1}}{d \phi^{\beta}} \\ &= \frac{\beta}{\beta + 1} \left[\frac{d \phi^{\beta+1}}{d \phi} \frac{d \phi}{d \phi^{\beta}} \right] = \frac{\beta}{\beta + 1} \left[\frac{d \phi^{\beta+1}}{d \phi} \left(\frac{d \phi^{\beta}}{d \phi} \right)^{-1} \right] \\ &= \frac{\beta}{\beta + 1} \left[(\beta + 1) \phi^{\beta} (\beta \phi^{\beta-1})^{-1} \right] = \frac{\beta}{\beta + 1} \left[\left(\frac{\beta + 1}{\beta} \right) \frac{\phi^{\beta}}{\phi^{\beta-1}} \right] = \phi \end{aligned} \quad (24)$$

Eq. (22) represents the type of fundamental nonlinear transformations used herein to obtain the generalized FD schemes corresponding with more general nonlinear fluxes. Further note that when $\beta = 1$, then ϕ above may take all real values, both negative and positive. An important observation is that a straightforward evaluation of Eq. (22) breaks down for the cases $\beta = 0$ and $\beta = -1$. In such instances, we take the respective limit and employ logarithmic substitutions

$$\lim_{\beta \rightarrow 0} \frac{\beta}{\beta + 1} \left[\left(\frac{\beta + 1}{\beta} \right) \frac{\phi^{\beta}}{\phi^{\beta-1}} \right] = \frac{1}{\phi^{-1}} = \left(\frac{d \log \phi}{d \phi} \right)^{-1} = \frac{d \phi}{d \log \phi} \quad (25)$$

$$\lim_{\beta \rightarrow -1} \frac{\beta}{\beta + 1} \left[\left(\frac{\beta + 1}{\beta} \right) \frac{\phi^{\beta}}{\phi^{\beta-1}} \right] = \phi^{-1} / \phi^{-2} = \left(-\frac{d \log(1/\phi)}{d(\phi)} \right) \left(-\frac{d \phi}{d(1/\phi)} \right) = \frac{d \log(1/\phi)}{d(1/\phi)} \quad (26)$$

recovering the type of transformation illustrated with reference to the Ranocha's mass flux.

Equation (22) therefore re-expresses ϕ in terms of a new parameterized function comprised of its derivatives, $\phi = f_{\bar{\phi}}(\beta)$. By substituting finite difference approximations, the limiting case of two-point derivatives obtains various discrete mean values:

1. $\beta = 1 \rightarrow$ Arithmetic mean:

$$f_{\bar{\phi}}(1) = \frac{1}{2} \frac{d \phi^2}{d \phi} \approx \frac{1}{2} \frac{\delta \phi^2}{\delta \phi} \rightarrow \frac{1}{2} \frac{\delta_{2pt} \phi^2}{\delta_{2pt} \phi} = \frac{1}{2} \frac{\phi_a^2 - \phi_b^2}{\phi_a - \phi_b} = \frac{\phi_a + \phi_b}{2} = \bar{\phi}$$

2. $\beta = \frac{1}{2}$ → Heronian mean:

$$f_{\bar{\phi}}(1/2) = \frac{1}{3} \frac{d\sqrt{\phi^3}}{d\sqrt{\phi}} \approx \frac{1}{3} \frac{\delta\sqrt{\phi^3}}{\delta\sqrt{\phi}} \rightarrow \frac{1}{3} \frac{\delta_{2\text{pt}}\sqrt{\phi^3}}{\delta_{2\text{pt}}\sqrt{\phi}} = \frac{1}{3} \frac{(\sqrt{\phi_a} - \sqrt{\phi_b})^3 + 3\phi_a\sqrt{\phi_b} - 3\phi_b\sqrt{\phi_a}}{\sqrt{\phi_a} - \sqrt{\phi_b}} = \frac{(\sqrt{\phi_a} - \sqrt{\phi_b})^2 + 3\sqrt{\phi_a}\sqrt{\phi_b}}{3} = \frac{\phi_a + \sqrt{\phi_a\phi_b} + \phi_b}{3} = \bar{\phi}^E$$

3. $\beta = 0$ → Logarithmic mean:

$$f_{\bar{\phi}}(0) = \frac{d\phi}{d \log \phi} \approx \frac{\delta\phi}{\delta \log \phi} \rightarrow \frac{\delta_{2\text{pt}}\phi}{\delta_{2\text{pt}} \log \phi} = \frac{\phi_a - \phi_b}{\log \phi_a - \log \phi_b} = \bar{\phi}^{(\log)}$$

4. $\beta = -\frac{1}{2}$ → Geometric mean:

$$f_{\bar{\phi}}(-1/2) = -\frac{d\sqrt{\phi}}{d(1/\sqrt{\phi})} \approx -\frac{\delta\sqrt{\phi}}{\delta(1/\sqrt{\phi})} \rightarrow \frac{\delta_{2\text{pt}}\sqrt{\phi}}{\delta_{2\text{pt}}(1/\sqrt{\phi})} = \frac{\sqrt{\phi_a} - \sqrt{\phi_b}}{\frac{1}{\sqrt{\phi_a}} - \frac{1}{\sqrt{\phi_b}}} = \sqrt{\phi_a\phi_b} = \bar{\phi}^G$$

5. $\beta = -1$ → "Harmonic-logarithmic" mean:

$$f_{\bar{\phi}}(-1) = \frac{d \log(1/\phi)}{d(1/\phi)} \approx \frac{\delta \log(1/\phi)}{\delta(1/\phi)} \rightarrow \frac{\delta_{2\text{pt}} \log(1/\phi)}{\delta_{2\text{pt}}(1/\phi)} = \frac{\log(1/\phi_a) - \log(1/\phi_b)}{\frac{1}{\phi_a} - \frac{1}{\phi_b}} = \bar{\phi}^{(H \log)}$$

6. $\beta = -2$ → Harmonic mean:

$$f_{\bar{\phi}}(-2) = 2 \frac{d\phi^{-1}}{d\phi^{-2}} \approx \frac{\delta\phi^{-1}}{\delta\phi^{-2}} \rightarrow \frac{\delta_{2\text{pt}}\phi^{-1}}{\delta_{2\text{pt}}\phi^{-2}} = \frac{\frac{1}{\phi_a} - \frac{1}{\phi_b}}{\frac{1}{\phi_a^2} - \frac{1}{\phi_b^2}} = 2 \frac{\phi_b\phi_a}{\phi_b + \phi_a} = \bar{\phi}^H$$

Note that in the case of two-point means, we have the property that $f_{\bar{\phi}}(\beta_a) > f_{\bar{\phi}}(\beta_b)$ when $\beta_a > \beta_b$ [46]. Also, specialized procedures for dealing with the risk of a singular denominator will furthermore be necessary in the case of the logarithmic-based means (e.g., Ismail/Roe's procedure [47]).

Equation (22) thus presents a general parameterized family of means based on derivatives⁶. In [46], the authors show how to express different means in terms of a quotient expressions comprised of integrals of ϕ . While the present work independently developed the current derivative-based representation, we acknowledge the previous work's guidance towards the generalization provided in Eq. (22).

The following section leverages the ability to explicitly generate nonlinear mean quantities such as the ones presented above in order to develop new entropy consistent methods that are finite-difference compatible. Specifically, we consider the following re-interpretation of the density and internal energy thermodynamic variables as part of re-writing their respective convective terms,

$$\left. \begin{aligned} \rho &= f_{\bar{\rho}}(\beta = 0) = \frac{d\rho}{d \log \rho} \\ e &= f_{\bar{e}}(\beta = -1) = \frac{d \log e^{-1}}{de^{-1}} \end{aligned} \right\} \rightarrow \left\{ \begin{aligned} \frac{\partial \rho u}{\partial x} &= \frac{\partial}{\partial x} \left(\frac{d\rho}{d \log \rho} u \right) \\ \frac{\partial \rho u e}{\partial x} &= \frac{\partial}{\partial x} \left(\frac{d\rho}{d \log \rho} u \frac{d \log e^{-1}}{de^{-1}} \right) \end{aligned} \right. \quad (27)$$

As will be shown in the following section, a direct FD treatment of these analytic forms results in discrete entropy conservation for the current calorically-perfect setting with entropy defined in Eq. (6).

⁶Another well-known family of means based on differences are the Stolarsky means [48, 49], which also coincide with some of the popular averages mentioned above (e.g., arithmetic, geometric, logarithmic).

4 A class of finite-difference entropy-conserving methods

In order to devise the FD-EC schemes, we first consider the entropy equation that results from contracting the entropy variables in Eq. (8) with the governing Euler system:

$$\begin{aligned}\mathcal{C}_{\rho s} &= w_\rho \cdot \mathcal{C}_\rho + \sum_{m=1}^d w_{\rho u_m} \cdot (\mathcal{C}_{\rho u_m} + \mathcal{P}_{\rho u_m}) + w_{\rho E} \cdot (\mathcal{C}_{\rho E} + \mathcal{P}_{\rho E}) \\ &= [s - \gamma c_v] \cdot \mathcal{C}_\rho + \frac{1}{T} \cdot (\mathcal{C}_{\rho e} + \mathcal{P}_{\rho e})\end{aligned}\quad (28)$$

Note that the above leverages the energy consistent relations from Eq. (4) and (5). The current intent is then to recover the entropy conservation statement by judiciously discretizing the primary system. To this end, we first assume a direct discretization of the respective convective and pressure terms previously given in Eqs. (1)–(5). The centered and biased FD stencil renditions for each term associated with the (n) direction derivative are given in the following Tables 1 and 2, where the \mathcal{C} and \mathcal{P} symbols can now refer to discrete representations based on the context. We allow for additional flexibility in how the density and internal energy will be defined via the specialized FD means presented in Section 3; the necessary forms for achieving exact entropy conservation are derived below. Note that the choice of \mathcal{C}_ρ automatically specifies the momentum treatment $\mathcal{C}_{\rho u}$ that is necessary for fulfilling kinetic-energy-preservation. As we presume a divergence like discretization of mass, the associated KEP form is that of Feiereisen [50].

Centered	
$\mathcal{C}_\rho^{(n)}$	$\delta_{x_n}^c (\tilde{\rho} u_n)$
$\mathcal{C}_{\rho u_m}^{(n)}$	$\frac{1}{2} [\delta_{x_n}^c (\tilde{\rho} u_n u_m) + \tilde{\rho} u_n \delta_{x_n}^c u_m + u_m \delta_{x_n}^c (\tilde{\rho} u_n)]$
$\mathcal{C}_{\rho e}^{(n)}$	$\delta_{x_n}^c (\tilde{\rho} u_n \tilde{e})$
$\mathcal{P}_{\rho u_m}^{(n)}$	$\delta_{x_m}^c p$ if $n = m$, otherwise 0
$\mathcal{P}_{\rho e}^{(n)}$	$p \delta_{x_n}^c u_n$

Table 1: Finite-difference discretization of Euler derivatives assuming SBP-compatible stencils. In the case of the FD-EC methods with central convective operators, $\mathcal{C}^{(n)}$, the auxiliary variables are $\tilde{\rho} \equiv \frac{\delta_{x_n}^c \rho}{\delta_{x_n}^c \log \rho} \triangleq \bar{\rho}^{(\log, n)}$ and $\tilde{e} \equiv \frac{\delta_{x_n}^c \log e^{-1}}{\delta_{x_n}^c e^{-1}} \triangleq \bar{e}^{(H \log, n)}$.

Biased	
$\mathcal{C}_\rho^{(\pm, n)}$	$\delta_{x_n}^\pm (\tilde{\rho} u_n)$
$\mathcal{C}_{\rho u_m}^{(\pm, n)}$	$\frac{1}{2} [\delta_{x_n}^\pm (\tilde{\rho} u_n u_m) + \tilde{\rho} u_n \delta_{x_n}^\mp u_m + u_m \delta_{x_n}^\pm (\tilde{\rho} u_n)]$
$\mathcal{C}_{\rho e}^{(\pm, n)}$	$\delta_{x_n}^\pm (\tilde{\rho} u_n \tilde{e})$
$\mathcal{P}_{\rho u_m}^{(\pm, n)}$	$\delta_{x_m}^\mp p$ if $n = m$, otherwise 0
$\mathcal{P}_{\rho e}^{(\pm, n)}$	$p \delta_{x_n}^\pm u_n$

Table 2: Finite-difference discretization of Euler derivatives assuming SBP-compatible stencils. In the case of the FD-EC methods with biased convective operators, $\mathcal{C}^{(\pm, n)}$, the auxiliary variables are $\tilde{\rho} \equiv \frac{\delta_{x_n}^\mp \rho}{\delta_{x_n}^\mp \log \rho} \triangleq \bar{\rho}^{(\log, \mp, n)}$ and $\tilde{e} \equiv \frac{\delta_{x_n}^\mp \log e^{-1}}{\delta_{x_n}^\mp e^{-1}} \triangleq \bar{e}^{(H \log, \mp, n)}$.

Entropy conservation is enforced by choosing $\tilde{\rho}$ and \tilde{e} such that any spurious volumetric terms are canceled and all that remain are consistent boundary terms. This is required in a point-wise manner in order to further guarantee *local* conservation in the discrete entropy dynamics. To see this, one employs the presumed form of the discretized convective and pressure terms while furthermore employing the calorically perfect gas assumptions with respect to the definition of entropy, as well as re-writing $1/T = c_v/e$; these manipulations yield the following (presented in one-dimension and the right-biased velocity rendition for simplicity):

$$\begin{aligned}
\mathbf{c}_{\rho s}|_{\partial\Omega} &= \int_{\Omega} \mathbf{c}_{\rho s} \\
&= \int_{\Omega} \left[\left[c_v \cdot \log \frac{e}{e_r} - c_v(\gamma - 1) \cdot \log \frac{\rho}{\rho_r} - \gamma c_v \right] \cdot \mathbf{C}_{\rho} + \frac{c_v}{e} \cdot (\mathbf{C}_{\rho e} + \mathcal{P}_{\rho e}) \right] \\
&= \underbrace{c_v \int_{\Omega} \left[\frac{1}{e} \cdot \mathcal{P}_{\rho e} - (\gamma - 1) \log \frac{\rho}{\rho_r} \cdot \mathbf{C}_{\rho} \right]}_{(1)} + \underbrace{c_v \int_{\Omega} \left[\left(\log \frac{e}{e_r} - \gamma \right) \cdot \mathbf{C}_{\rho} + \frac{1}{e} \cdot \mathbf{C}_{\rho e} \right]}_{(2)}
\end{aligned} \tag{29}$$

In terms of variable units, the explicit normalization of internal energy and density by their reference quantities within the logarithmic expressions of entropy have now been included for clarity of presentation. As an example, we show this below in Eqs. (30) and (31) for the one-dimensional case assuming a set of biased operators (note that the same mechanics apply for the opposite biasing and for the central stencils as well). The integral notation used below actually implies summation across nodal points in the discrete setting according to the SBP diagonal norm that encodes the interface flux spacings [41]

$$\begin{aligned}
\underbrace{c_v \int_{\Omega} \left[\frac{1}{e} \cdot \mathcal{P}_{\rho e}^{(+)} - (\gamma - 1) \log \frac{\rho}{\rho_r} \cdot \mathbf{C}_{\rho}^{(+)} \right]}_{(1)} : & \quad c_v \int_{\Omega} \left[e^{-1} p \cdot \delta_x^+ u - (\gamma - 1) \log \frac{\rho}{\rho_r} \cdot \delta_x^+ (\tilde{\rho} u) \right] \\
&= c_v(\gamma - 1) \int_{\Omega} \left[\rho \cdot \delta_x^+ u - \log \frac{\rho}{\rho_r} \cdot \delta_x^+ (\tilde{\rho} u) \right] \\
&= c_v(\gamma - 1) \left[\rho u - \log \frac{\rho}{\rho_r} \cdot \tilde{\rho} u \right] |_{\partial\Omega} \\
&\quad - c_v(\gamma - 1) \int_{\Omega} u \underbrace{\left[\delta_x^- \rho - \tilde{\rho} \cdot \delta_x^- \left(\log \frac{\rho}{\rho_r} \right) \right]}_{\text{need}=0}
\end{aligned} \tag{30}$$

$$\begin{aligned}
\underbrace{c_v \int_{\Omega} \left[\left(\log \frac{e}{e_r} - \gamma \right) \cdot \mathbf{C}_{\rho}^{(+)} + \frac{1}{e} \cdot \mathbf{C}_{\rho e}^{(+)} \right]}_{(2)} : & \quad c_v \int_{\Omega} \left[\left(\log \frac{e}{e_r} - \gamma \right) \cdot \delta_x^+ (\tilde{\rho} u) + e^{-1} \cdot \delta_x^+ (\tilde{\rho} u \tilde{e}) \right] \\
&= c_v \left[\left(\log \frac{e}{e_r} - \gamma \right) \cdot (\tilde{\rho} u) + e^{-1} \cdot (\tilde{\rho} u \tilde{e}) \right] |_{\partial\Omega} \\
&\quad - c_v \int_{\Omega} \tilde{\rho} u \underbrace{\left[-\delta_x^- \left(\log \frac{e^{-1}}{e_r^{-1}} \right) + \tilde{e} \cdot \delta_x^- e^{-1} \right]}_{\text{need}=0}
\end{aligned} \tag{31}$$

The exposition above in Eqs. (30) and (31) places no stipulations on the order of the difference operators and only requires the SBP property and the use of dual operators in the case of biased stencils. Also, while the current example is shown for a single dimension, it should be understood that the set of specialized mean quantities $\tilde{\rho}$ and \tilde{e} will need to be calculated for each directional derivative (see Remark 3).

The boundary surface estimates are based on the extrapolation formulas associated with the SBP operators per Eq. (11) and (12). From the SBP manipulations in Eqs. (30) and (31), one can identify the consistent entropy boundary terms that are induced by the resulting FD scheme. For example, with respect to the left boundary one can re-arrange terms to

recover the associated high-order consistent entropy flux

$$\mathcal{C}_{\rho s}|_{\ell} \equiv \mathcal{F}_{\rho s, \ell} = \overbrace{\left(\tilde{\rho} u \right)_{\ell} \cdot \left(c_v \left(\log \frac{e}{e_r} \right)_{\ell} - c_v (\gamma - 1) \left(\log \frac{\rho}{\rho_r} \right)_{\ell} \right)}^{(\rho u s)_{\ell}} + \underbrace{\gamma c_v (\rho_{\ell} u_{\ell} - (\tilde{\rho} u)_{\ell}) - c_v (\rho_{\ell} u_{\ell} - (\tilde{\rho} u \tilde{e})_{\ell} (e^{-1})_{\ell})}_{O(\Delta x^p)} \quad (32)$$

Equation (32) is valid for all of the SBP stencils—whether central or forward/backward biased. We further note that in cases where $\tilde{\rho} \neq \rho$ and $\tilde{e} \neq e$ (as will be the case for the resulting EC schemes) then the resulting boundary flux includes a persistent zero-consistent component.

The spurious entropy volumetric terms that result from the summation-by-parts manipulations in Eqs. (30) and (31) are canceled *point-wise* by selecting the auxiliary variables $\tilde{\rho} \equiv \frac{\delta_x^- \rho}{\delta_x^- \log \rho} \triangleq \bar{\rho}^{(\log, -)}$ and $\tilde{e} \equiv \frac{\delta_x^- \log e^{-1}}{\delta_x^- e^{-1}} \triangleq \bar{e}^{(H \log, -)}$. Per the discussion of Section 3, these new variables constitute specialized averages of the density and internal energy. The resulting method is then successfully entropy conserving and can also be associated with a local entropy-conserving Tadmor-type flux condition (see Remark 2). In addition to being entropy conserving, it is also kinetic-energy-preserving by construction and can be shown to be pressure-equilibrium-preserving (PEP) as discussed in Section 4.1. The finite difference representation that is induced in the discrete entropy equation can be identified from the structure of the boundary flux in Eq. (32). Specifically, the forward biased rendition gives

$$\mathcal{C}_{\rho s}^{(+)} = s \delta_x^+ (\tilde{\rho} u) + \tilde{\rho} u \delta_x^- s + \underbrace{\left[c_v (\gamma - 1) \cdot (\rho \delta_x^+ u + u \delta_x^- \rho) - \gamma c_v \cdot \delta_x^+ (\tilde{\rho} u) + c_v (e^{-1} \delta_x^+ (\tilde{\rho} u \tilde{e}) + \tilde{\rho} u \tilde{e} \delta_x^- e^{-1}) \right]}_{O(\Delta x)^p} \quad (33)$$

Thus we recover a split form in the entropy dynamics that is based on the special nonlinear averages $\tilde{\rho}$ and \tilde{e} ; and besides the main entropy terms, there is furthermore a zero-consistent correction. Note that analogous expressions arise when switching the biasing and also when using the central operators (not shown).

Remark 1 *The groupings identified in Eq. (29) for achieving point-wise cancellations of the spurious entropy dynamics are non-unique and can lead to different EC methods. This flexibility in scheme design is an advantageous characteristic of the proposed FD-EC methodology. The current choice of groupings results in definitions for $\tilde{\rho}$ and \tilde{e} that are solely functions of density and internal energy, respectively.*

Remark 2 *The point-wise cancellations of the spurious dynamics in the discrete entropy equation (see Eqs. (30)–(31)) suggest that the FD-EC schemes also satisfy the following Tadmor-type EC flux condition: $\sum_{m=1}^{2+d} (w_{m, i+1} - w_{m, i}) \mathcal{F}_{m, i+1/2}^{(n)} = (\tilde{\psi}_{i+1}^{(n)} - \tilde{\psi}_i^{(n)})$ for $i = 1, \dots, N - 1$, where $\tilde{\psi}_1^{(n)} \equiv \tilde{\psi}_{\ell}^{(n)} = (\sum_m^{2+d} w_{m, 1} \mathcal{F}_{m, \ell}^{(n)} - \mathcal{F}_{\rho s, \ell}^{(n)})$ (see Section 3.2.1 in [41]).*

Remark 3 *The specialized auxiliary variables $\tilde{\rho}$ and \tilde{e} need to be calculated with respect to each directional derivative.*

For example, fluxes in the n direction would require calculating $\tilde{\rho}^{(\pm, n)} \triangleq \frac{\delta_{x_n}^{\pm} \rho}{\delta_{x_n}^{\pm} \log \rho} \equiv \bar{\rho}^{(\log, \pm, n)}$ and $\tilde{e}^{(\pm, n)} \triangleq \frac{\delta_{x_n}^{\pm} \log e^{-1}}{\delta_{x_n}^{\pm} e^{-1}} \equiv \bar{e}^{(H \log, \pm, n)}$ in the biased case.

The resulting FD-EC scheme is conservative and induces a local flux form. The recursive procedure from Eq. (14) may be used to recover the associated interface fluxes of the primary system upon first supplying the boundary fluxes⁷, which are the following for the proposed split form (here focusing on the left boundary for brevity):

$$\mathcal{F}_{\ell}^{(n)} = \begin{bmatrix} \mathcal{F}_{\rho} \\ \mathcal{F}_{\rho u_m} \\ \mathcal{F}_{\rho E} \end{bmatrix}_{\ell}^{(n)} = \begin{bmatrix} (\tilde{\rho} u_n)_{\ell} \\ \frac{1}{2} (\tilde{\rho} u_n u_m)_{\ell} + \frac{1}{2} (\tilde{\rho} u_n)_{\ell} (u_m)_{\ell} + \delta_{mn} \cdot p_{\ell} \\ \frac{1}{2} \sum_{m=1}^d (u_m)_{\ell} (\tilde{\rho} u_n u_m)_{\ell} + (\tilde{\rho} u_n \tilde{e})_{\ell} + (u_n)_{\ell} p_{\ell} \end{bmatrix} \quad (34)$$

These boundary fluxes may further be used to employ necessary boundary and block interface coupling via Simultaneous Approximation Terms (SATs) [33].

⁷Recall that in most cases, Eq. (4) is just an evaluation of the flux at the boundary nodes and that only generalized SBP operators [32] feature specialized boundary extrapolation operators that would yield the split-form averaging of the flux at the boundary.

It is insightful to also observe the structure of the resulting fluxes on the domain interior. For example, the two-point central difference stencils give the following “wide-width” interior interface fluxes

$$\begin{aligned}
& \left(\mathcal{C}^{(n)} + \mathcal{P}^{(n)} \right)_{2\text{pt}} \\
\rightarrow \mathcal{F}_{i+1/2}^{(n)}|_{\text{wide}} = & \left[\begin{aligned} & \frac{1}{2} \overline{(\rho_i, \rho_{i+2})}^{\log, n} u_{i+1} + \frac{1}{2} \overline{(\rho_{i-1}, \rho_{i+1})}^{\log, n} u_i \\ & \mathcal{F}_{\rho, i+1/2}^{(n)} \cdot \frac{(u_{m, i+1} + u_{m, i})}{2} + \delta_{mn} \cdot \frac{p_{i+1} + p_i}{2} \\ & \mathcal{F}_{\rho, i+1/2}^{(n)} \cdot \sum_{m=1}^d \frac{u_{m, i} u_{m, i+1}}{2} \\ & + \frac{1}{2} \overline{(\rho_i, \rho_{i+2})}^{\log, n} u_{i+1} \overline{(e_i, e_{i+2})}^{H \log, n} \\ & + \frac{1}{2} \overline{(\rho_{i-1}, \rho_{i+1})}^{\log, n} u_i \overline{(e_{i-1}, e_{i+1})}^{H \log, n} \\ & + \frac{u_{n, i} p_{n, i+1} + u_{n, i+1} p_{n, i}}{2} \end{aligned} \right] \quad (35)
\end{aligned}$$

and the two-point biased difference stencils yield the following parameterized “narrow-width” interior interface fluxes

$$\begin{aligned}
& \alpha \cdot \left(\mathcal{C}^{(n, +)} + \mathcal{P}^{(n, +)} \right)_{2\text{pt}} + (1 - \alpha) \cdot \left(\mathcal{C}^{(n, -)} + \mathcal{P}^{(n, -)} \right)_{2\text{pt}} \\
\rightarrow \mathcal{F}_{i+1/2}^{(n)}|_{\text{narrow}}^\alpha = & \left[\begin{aligned} & \overline{(\rho_i, \rho_{i+1})}^{\log, n} \left((1 - \alpha) \cdot u_{n, i} + \alpha \cdot u_{n, i+1} \right) \\ & \mathcal{F}_{\rho, i+1/2}^{(n)} \cdot \frac{(u_{m, i+1} + u_{m, i})}{2} + \delta_{mn} \cdot \left((1 - \alpha) \cdot p_{i+1} + \alpha \cdot p_i \right) \\ & \mathcal{F}_{\rho, i+1/2}^{(n)} \cdot \left(\sum_{m=1}^d \frac{u_{m, i} u_{m, i+1}}{2} + \overline{(e_i, e_{i+1})}^{H \log, n} \right) \\ & + (1 - \alpha) \cdot u_{n, i} p_{i+1} + \alpha \cdot u_{n, i+1} p_i \end{aligned} \right] \quad (36)
\end{aligned}$$

In the above, the arguments of the nonlinear averages computed in the n direction are explicitly written for additional clarity. Note that while the two-point wide scheme stems from two-point differences, the resulting flux is multi-point.

Some interesting insights transpire from studying the interior flux forms stemming from the two-point schemes. First, we note that the central stencils induce a wider node dependence and furthermore that their fluxes couple the thermodynamic interface reconstructions with that of the transport velocity. On the other hand, the biased stencils—at least in the two-point scenario—split up these variable reconstructions. Next, we note that the biased stencils yield counter-balanced biasing in the flux with respect to velocity and pressure when $\alpha \neq 1/2$. The associated interface reconstructions in such cases is of lower order than the symmetric case ($\alpha = 1/2$, as expected by the fact that such biased stencils are typically one order lower than their centered counterparts. To the authors’ knowledge, this is the first time that EC fluxes with biased interior quantities have been presented, and leveraging such properties toward improving the scheme resolution of sharp gradients constitutes a line of future research.

Also notable upon studying these interior fluxes is the fact that a symmetric combination of the biased two-point operators with $\alpha = 1/2$ recovers the second-order flux of Ranocha [25, 26], therefore formalizing its finite-difference compatibility. This exact congruence between the symmetric two-point narrow-width schemes and the Ranocha flux is not expected to hold to high-order, however. Namely, the Ranocha flux (as well as other two-point EC fluxes in the literature [51, 52]) is typically extended to high-order via flux-differencing [16, 41], which is a Richardson-type extrapolation of the low-order two-point fluxes. This, however, need not be the case for the current FD-EC methods which can technically be extended to high-order simply by considering multi-point FD stencils in the definitions of $\tilde{\rho}$ and \tilde{e} as well as the flux derivatives. This is exemplified most simply when inspecting the mass flux term, which motivates the general uniqueness of the respective representations at high order. Assuming a K -width central stencil

with p -point biasing for the associated dual pair schemes, one would have

(via current FD-EC wide):

$$\begin{aligned}
& \mathcal{F}_{\rho, i+1/2}^{(n)} - \mathcal{F}_{\rho, i-1/2}^{(n)} \\
&= \sum_{k=-K}^K d_{i, i+k}^c \cdot \left[\tilde{\rho}_{i+k}^{(n)} \cdot u_{n, i+k} \right] \\
&= \sum_{k=-K}^K d_{i, i+k}^c \cdot \left[\tilde{\rho}_i^{(n)} \cdot u_{n, i} + \tilde{\rho}_{i+k}^{(n)} \cdot u_{n, i+k} \right] \\
&= \sum_{k=-K}^K d_{i, i+k}^c \cdot \left[\overline{(\rho_{i+k-K}, \dots, \rho_{i+k+K})}^{\log, n} \cdot u_{n, i+k} \right]
\end{aligned} \tag{37}$$

(via current FD-EC symmetric narrow, $\alpha = 1/2$):

$$\begin{aligned}
& \mathcal{F}_{\rho, i+1/2}^{(n)} - \mathcal{F}_{\rho, i-1/2}^{(n)} \\
&= \sum_{k=-K}^K \frac{1}{2} \left(d_{i, i+k}^+ \cdot \tilde{\rho}_{i+k}^{(n, -)} + d_{i, i+k}^- \cdot \tilde{\rho}_{i+k}^{(n, +)} \right) \cdot u_{n, i+k} \\
&= \sum_{k=-K}^K \frac{1}{2} \left(d_{i, i+k}^+ \cdot \left[\tilde{\rho}_i^{(n, -)} \cdot u_{n, i} + \tilde{\rho}_{i+k}^{(n, -)} \cdot u_{n, i+k} \right] + d_{i, i+k}^- \cdot \left[\tilde{\rho}_i^{(n, +)} \cdot u_{n, i} + \tilde{\rho}_{i+k}^{(n, +)} \cdot u_{n, i+k} \right] \right) \\
&= \sum_{k=-K}^K \frac{1}{2} \left(d_{i, i+k}^+ \cdot \overline{(\rho_{i+k-K}, \dots, \rho_{i+k+K-p})}^{\log, n} + d_{i, i+k}^- \cdot \overline{(\rho_{i+k-K+p}, \dots, \rho_{i+k+K})}^{\log, n} \right) \cdot u_{n, i+k}
\end{aligned} \tag{38}$$

(via two-point flux-differencing):

$$\begin{aligned}
& \mathcal{F}_{\rho, i+1/2}^{(n)} - \mathcal{F}_{\rho, i-1/2}^{(n)} \\
&= \sum_{k=-K}^K d_{i, i+k}^c \cdot \left[\overline{(\rho_i, \rho_{i+k})}^{\log, n} \cdot (u_{n, i} + u_{n, i+k}) \right]
\end{aligned} \tag{39}$$

where in the above we have the following relations for the stencil coefficients

$$\sum_k d_{i, i+k}^c = \sum_k d_{i, i+k}^\pm = 0 \quad \text{and} \quad \frac{(d_{i, i+k}^+ + d_{i, i+k}^-)}{2} = d_{i, i+k}^c \tag{40}$$

and where

$$\text{(on the interior)} : \quad d_{i, i-k}^c = -d_{i, i+k}^c \quad \text{and} \quad d_{i, i}^c = 0. \tag{41}$$

Note that Eqs. (37) and (38) are still expressed in a flux-difference flavor (albeit with multi-point information), which stems naturally from their finite difference origins. Due to the nonlinearity of the logarithmic mean, it is clear that the standard flux-differenced implementation of Ranocha's method will differ from the newly-presented symmetric narrow-width method for $K \neq 1$, as the latter would utilize a multi-point logarithmic means of density rather than two-point logarithmic means. Suitable algorithms for handling such multi-point nonlinear averages near singular points (i.e., where the quotient formulas from Section 2 are near zero) are still under development; therefore, the numerical results in the following section will focus on the class of two-point FD-EC methods. Appendix A, however, provides an alternate error-reducing treatment for the narrow biased schemes based on flux differencing with multi-point difference stencils.

4.1 On the kinetic-energy and pressure-equilibrium preservation of the new schemes

Besides being entropy conserving, the new methods feature additional robustness-promoting characteristics—namely, kinetic-energy and pressure-equilibrium preservation. These are briefly described here.

The FD-EC methods employ splittings for the mass and momentum equations that yield the kinetic energy preserving (KEP) formulation of Feiereisen [50], wherein no spurious convective dynamics are induced in the associated discrete

secondary equation. For example, the centered representation gives

$$\begin{aligned} \mathcal{C}_{\rho k} &= \sum_{m=1}^d \left[u_m \mathcal{C}_{\rho u_m} - \frac{1}{2} u_m^2 \mathcal{C}_{\rho} \right] \\ \text{(centered)} &= \frac{1}{2} [u_m \delta_{x_n} (\tilde{\rho} u_n u_m) + \tilde{\rho} u_n u_m \delta_{x_n} u_m] \\ &\xrightarrow{(2pt)} \mathcal{F}_{\rho k, i+1/2}^{(n)} = \frac{1}{4} [(\tilde{\rho} u_n u_m)_i (u_m)_{i+1} + (\tilde{\rho} u_n u_m)_{i+1} (u_m)_i] \end{aligned} \quad (42)$$

We note that the convective term in the kinetic energy equation is in a quadratically split form which will result in local conservation of the quantities. Analogous expressions can be written for the biased stencils. Although kinetic energy preservation does not provide a rigorous nonlinear stability metric for compressible flows, incorporating its numerical consistency has been shown to greatly enhance solution quality—even for the class of entropy conserving Tadmor fluxes [51, 27]. And as motivated in Eqs. (5) and (10) of Section 2, it forms a key consistency within the continuous entropy analysis.

Next, it is possible to also show that all the new FD-EC schemes have the Pressure Equilibrium Preservation (PEP) property [4, 26, 53] for the current context of a calorically-perfect single fluid. In other words, they have the ability to preserve the equilibrium of velocity and pressure across an interface. The condition on the discretization of the momentum equation assuming constant velocity U_o and pressure P_o (see [53, 26]) is that the momentum flux is equal to

$$\mathcal{F}_{\rho u_m, i+1/2} = \mathcal{F}_{\rho, i+1/2} \cdot U_o + \text{const}(U_o, P_o). \quad (43)$$

This is clearly satisfied by the schemes considered—for example, see Eqs. (35) and (36). The other condition, on the internal-energy flux, is that it should be a constant dependent only on the values of U_o and P_o [53]:

$$\mathcal{F}_{\rho e, i+1/2} = \text{const}(U_o, P_o). \quad (44)$$

This is clearly the case for the pressure-velocity term in internal energy ($p \delta_{x_n} u$) and it is also true for the convective flux since

$$\mathcal{F}_{\rho e, i+1/2}^{(n, \text{conv})} = \bar{\rho}^{(\log)} (\bar{\rho}^{-1})^{(\log)} U_o = \bar{\rho}^{(\log)} (\bar{\rho}^{(\log)})^{-1} \frac{P_o U_o}{\gamma - 1}. \quad (45)$$

The ability to appropriately preserve such equilibrium conditions across interfaces is essential towards avoiding the numerical instigation of solution instabilities that can threaten both numerical robustness and solution quality [54, 9].

5 Numerical results

The new EC schemes are here tested with a variety of cases (i.e., the 2D isentropic vortex, the 1D density wave, the 1D Sod shock tube, and the 3D Taylor Green vortex) in order to verify the validity of the theoretical results. In particular, we consider the new scheme based on the wide stencil presented in Eq. (35), here referred to as EC^W, and three schemes from the family identified in Eq. (36), that with $\alpha = 0$, $\alpha = 1$, and $\alpha = 0.5$ are labeled EC^B, EC^F, and EC^S, respectively. Notably, EC^S is analogous to the scheme of Ranocha in the scenario of a two-point second order stencil. A summary of the schemes and their respective numerical fluxes is presented in Table 3.

Despite having demonstrated the capability to obtain high-order formulations of the presented EC schemes, the methods will all be tested with their low-order version, employing first and second order accurate differential operators. This is due to the singularity problem that occurs when evaluating the logarithmic mean for almost identical values. This challenge is handled in the case of two-point means by employing suitable expansion approximations such as the one famously introduced by Ismail and Roe [47]. Other similar approaches have been recently employed to produce schemes that are asymptotically entropy conserving [24, 28]. However, a generalization of the procedure for multiple-point means has yet to be developed.

The results presented in this section have been generated based on the flux forms of the FD schemes in the code STREAmS-2 [55]. Density, momentum and total energy are employed as the primary variables. All time integrations have been performed using the classical explicit fourth-order Runge-Kutta (RK4) scheme. In order to analyze the conservation properties of the schemes, we introduce the notation of using the angular brackets to indicate integration over the spatial domain $\langle \phi \rangle = \int_{\Omega} \phi d\Omega$ and using ϵ for the nondimensionalization $\epsilon_{\phi} = (\langle \phi \rangle - \langle \phi_0 \rangle) / |\langle \phi_0 \rangle|$, in which ϕ_0 indicates the values at the starting time. For all the simulations, the value for the normalized specific heat capacity at constant volume is $c_v = 1$ and $\gamma = 1.4$.

Ref.	\mathcal{F}_ρ	$\mathcal{F}_{\rho u_m, i+1/2}$	$\mathcal{F}_{\rho E}$
EC ^B new	$\overline{(\rho_i, \rho_{i+1})}^{(\log)} u_{n,i}$	$\mathcal{F}_\rho \overline{u_m} + p_{i+1}$	$\mathcal{F}_\rho \overline{(e_i, e_{i+1})}^{(H \log)} + \mathcal{F}_\rho \sum_m \frac{u_{m,i} u_{m,i+1}}{2} + p_{i+1} u_{n,i}$
EC ^F new	$\overline{(\rho_i, \rho_{i+1})}^{(\log)} u_{n,i+1}$	$\mathcal{F}_\rho \overline{u_m} + p_i$	$\mathcal{F}_\rho \overline{(e_i, e_{i+1})}^{(H \log)} + \mathcal{F}_\rho \sum_m \frac{u_{m,i} u_{m,i+1}}{2} + p_i u_{n,i+1}$
EC ^S [51]	$\overline{(\rho_i, \rho_{i+1})}^{(\log)} \overline{u_n}$	$\mathcal{F}_\rho \overline{u_m} + \overline{p}$	$\mathcal{F}_\rho \overline{(e_i, e_{i+1})}^{(H \log)} + \mathcal{F}_\rho \sum_m \frac{u_{m,i} u_{m,i+1}}{2} + \overline{(p, u)}$
EC ^W new	$0.5 \overline{(\rho_{i-1}, \rho_{i+1})}^{(\log)} u_{n,i}$ $+ 0.5 \overline{(\rho_i, \rho_{i+2})}^{(\log)} u_{n,i+1}$	$\mathcal{F}_\rho \overline{u_m} + \overline{p}$	$0.5 \overline{(\rho_{i-1}, \rho_{i+1})}^{(\log)} u_{n,i} \overline{(e_{i-1}, e_{i+1})}^{(H \log)}$ $+ 0.5 \overline{(\rho_i, \rho_{i+2})}^{(\log)} u_{n,i+1} \overline{(e_i, e_{i+2})}^{(H \log)}$ $+ \mathcal{F}_\rho \sum_m \frac{u_{m,i} u_{m,i+1}}{2} + \overline{(p, u)}$

Table 3: Numerical fluxes for the schemes used for the tests. The fluxes are evaluated along direction n at location $i + 1/2$. All interpolation operation are implicitly interpreted to be in the same direction n .

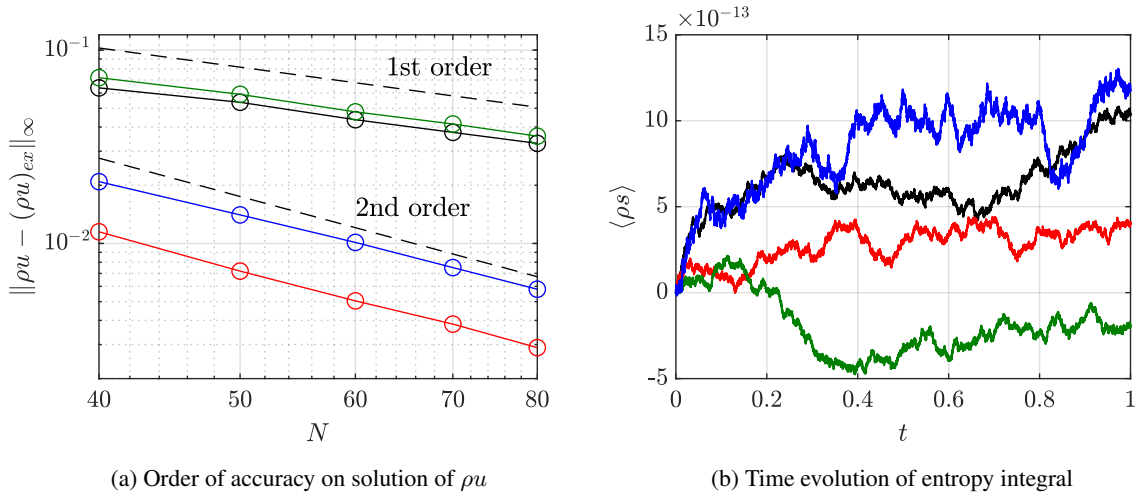


Figure 1: Isentropic vortex test for different discretizations: black lines are used for EC^B, red for EC^S, green for EC^F, blue EC^W. CFL = 0.01.

5.1 2D isentropic vortex

The two-dimensional isentropic Euler vortex problem has initial conditions

$$\begin{aligned} \frac{u(x, y)}{u_\infty} &= 1 - \frac{M_v}{M_\infty} \frac{y - y_0}{r_v} e^{(1-\hat{r}^2)/2} \\ \frac{v(x, y)}{u_\infty} &= \frac{M_v}{M_\infty} \frac{x - x_0}{r_v} e^{(1-\hat{r}^2)/2} \\ \frac{T(x, y)}{T_\infty} &= \left(\frac{p(x, y)}{p_\infty} \right)^{(\gamma-1)/\gamma} = \left(\frac{\rho(x, y)}{\rho_\infty} \right)^{\gamma-1} = 1 - \frac{\gamma-1}{2} M_v^2 e^{1-\hat{r}^2} \end{aligned}$$

in which $\hat{r} = r/r_v$ with core radius $r_v = 1/15$ and r is the distance from the vortex center. The characteristic values of velocity, density, and temperature are $u_\infty = 1$, $\rho_\infty = 1$, $T_\infty = 720 M_v r_v$, while pressure is derived from density as $p = \rho^\gamma / (\gamma M_\infty^2)$. The mean flow Mach number is $M_\infty = 0.5$ and the vortex, whose center is initially at coordinates $(x_0, y_0) = (0.5, 0.5)$, has a strength $M_v = 0.5$. The vortex core is $\rho(x_0, y_0) = 0.6941 \rho_\infty$; a non-negligible perturbation that is meant to instigate nonlinear effects. A 30×30 discretization is used for the square domain of unitary side with a uniform Cartesian grid; boundary conditions are periodic in all directions. Upon choosing to identify the vortex width as the point where $\rho/\rho_\infty = 0.99$, then approximately eight vortex widths can be said to fit along the length of the domain. The Courant number of the tests is set to CFL = 0.001, corresponding to a time step size $\Delta t = 2 \times 10^{-5}$. A full loop of the domain (i.e., approximately eight vortex widths) occurs each $t = 1$.

The isentropic vortex flow is an exact solution of the inviscid compressible flow equations and as such it can be used to evaluate the accuracy of the numerical methods. In Fig. 1a the error on momentum along the x axis is displayed as a function of N number of nodes in each direction. The error is evaluated as the maximum norm of the difference between the computed and the exact solution for momentum along the x direction $\|\rho u - (\rho u)_{ex}\|_\infty$, evaluated at a time $t = 0.01$ with CFL = 0.01. The analysis shows a difference between the first-order accurate (EC^F and EC^B) and the second-order accurate (EC^S and EC^W) methods. The reason behind this behaviour is easily explained by the fact that EC^F and EC^B use an asymmetrical numerical derivative for the discretization of the pressure term and an asymmetrical interpolator for velocity as well; on the other hand both EC^S and EC^W result in central schemes. Identical trends are witnessed upon inspecting the error of other quantities (not shown), such as the primitive variables (ρ, u, T) .

Despite this difference on the order of accuracy, all the schemes are able to exactly conserve entropy in a discrete sense, with an error in the conservation of the order of machine zero. The methods present very similar behavior, with a slightly larger drift observed in the asymmetric schemes.

5.2 1D density wave

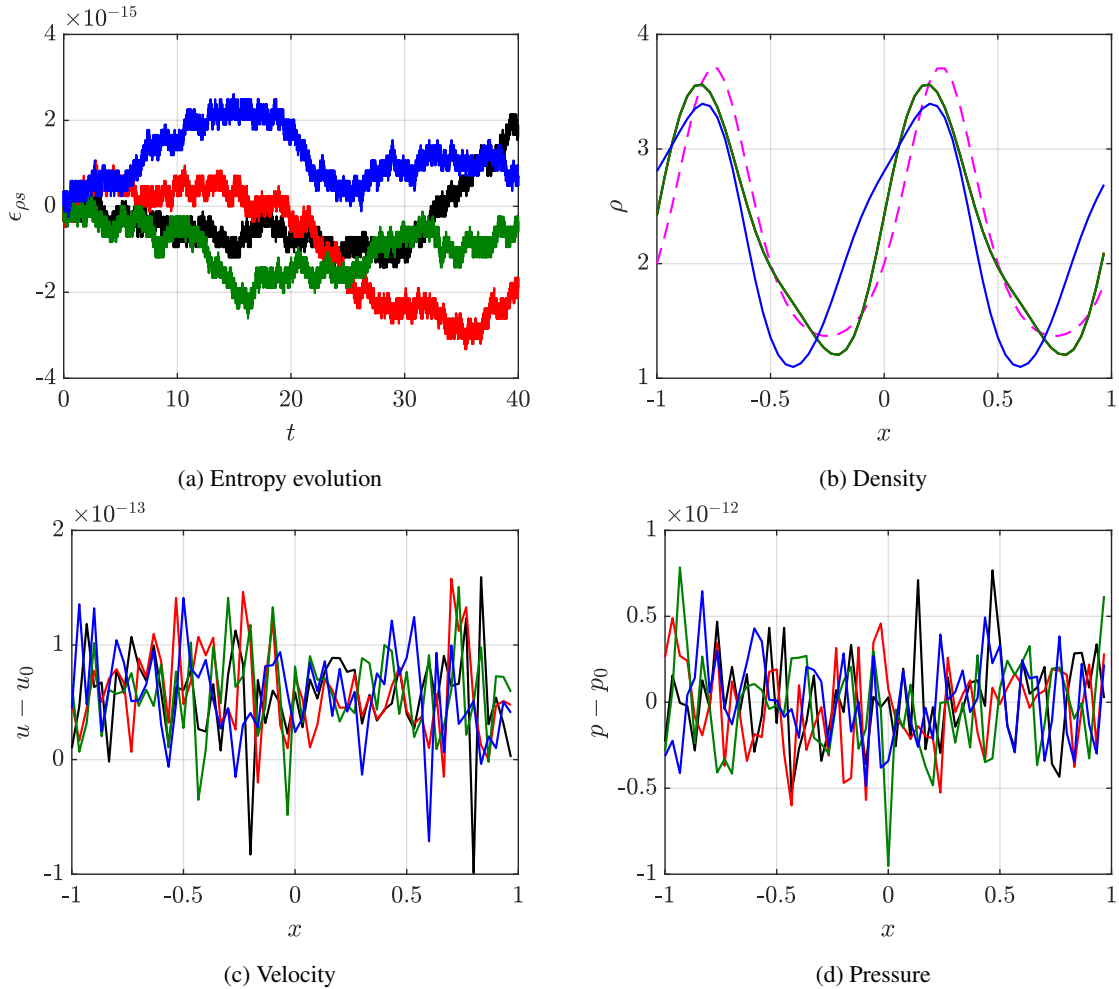


Figure 2: Density wave test for different discretizations: black lines are used for EC^B , red for EC^S , green for EC^F , blue EC^W ; dashed magenta line is the exact solution. CFL = 0.01, final solutions at $T = 40$.

It can be shown theoretically (see Section 4.1) that all of the current schemes have the PEP property. The simulation of a traveling density wave is well suited to numerically test the PEP property of the schemes. The initial conditions for the test are

$$\rho_0 = 1 + \exp\left(\sin\left(\frac{2\pi x}{L}\right)\right), \quad u_0 = 1, \quad p_0 = 1,$$

with the domain $[-L, L]$ with $L = 1$ discretized in 61 points and periodic boundary conditions. The Courant number has been chosen to be $CFL = 0.001$ to prevent errors on entropy conservation due to the temporal integrator, and the simulation has been carried out until a final time $T = 40$, which corresponds to approximately 20 cycles of the wave through the domain.

The simulation of the density wave also confirms the schemes' ability to exactly conserve global entropy (see Fig.2a). The theoretical prediction that the schemes would be PEP has also been confirmed: the errors introduced on velocity u and pressure p remain at machine precision even at the final time, as shown in Figs. 2c–d. For this test, the results produced by the two-point schemes (EC^B , EC^F , and EC^S) are indistinguishable, as shown for the density in Fig. 2b. This is due to the fact that the only difference between these methods is in the interpolation of u and p , which becomes irrelevant when they are constant throughout the domain. On the other hand, the results obtained with the scheme EC^W are appreciably different, which is likely a consequence of the wider stencil.

5.3 1D Sod shock tube

While the EC schemes have been derived in the hypothesis of smooth flows, it is important to observe their behavior in the presence of discontinuities, as this pushes the limits of the non-dissipative methods. When applied in shocked regions, these schemes will still conserve entropy, although producing non-physical oscillations.

In this vein, the Sod shock tube test is considered. The initial conditions upstream (U) and downstream (D) of the diaphragm, which is located at midpoint of the domain, are given by

$$\begin{aligned} \rho_U &= 1; & u_U &= 0; & p_U &= 1; \\ \rho_D &= 0.125; & u_D &= 0; & p_D &= 0.1. \end{aligned}$$

The simulation is carried out until $T = 0.1$ with $CFL = 0.01$ based on velocity $u_\infty = \sqrt{p_U/\rho_U}$. For the discretization of the interval $[-0.25, 0.25]$ 101 nodes are employed, however a much larger domain has been used to prevent the periodic boundary conditions to have any effect on the solution.

In Fig. 3, the solutions obtained with the various EC schemes are compared with the analytical one obtained with an exact Riemann solver. As expected, all the schemes are entropy conserving and generate spurious oscillations in the solution. As visible in Fig. 3c, none of the schemes are able to reproduce the correct behavior for entropy in the region leading up to shock $x \in [0.1, 0.2]$, and EC^W seems to present more oscillations. This behavior has been observed before for the scheme of Ranocha [26] (here EC^S) in [31]. This region is also one in which the oscillations are stronger for all the schemes when other variables are considered (e.g., density, velocity, temperature, pressure).

On the other hand, in the region $x \in [0, 0.1]$ the asymmetric schemes EC^B and EC^F present oscillations with smaller amplitude when compared to the central schemes EC^W and EC^S . This is particularly evident when inspecting velocity in Fig. 3b, for which a larger spike is present near $x = 0$ for the EC^S scheme. Such behavior further motivates interest in studying these biased schemes for use in flows exhibiting sharp gradients.

5.4 3D Taylor Green vortex

The inviscid Taylor Green vortex is used to test the schemes in a three-dimensional setting that serves as a benchmark for turbulence simulations; it generates smaller and smaller scales through vortex stretching. The initial conditions are given by

$$\begin{aligned} \rho(x, y, z) &= 1 \\ u(x, y, z) &= \sin(x) \cos(y) \cos(z) \\ v(x, y, z) &= -\cos(x) \sin(y) \cos(z) \\ w(x, y, z) &= 0 \\ p(x, y, z) &= 100 + \frac{(\cos(2x) + \cos(2y))(\cos(2x) + 2) - 2}{16} \end{aligned}$$

which correspond to a Mach number $M \approx 0.08$. The domain is a triperiodic cube of length 2π and it is discretized using $32 \times 32 \times 32$ nodes. The final time of the simulation is $T = 70$ and the time step size adapts to keep $CFL = 0.01$.

Entropy is conserved for the test case (Fig. 4a), but, while for the central schemes EC^W and EC^S the error is down to 10^{-14} , for the asymmetric schemes EC^B and EC^F there is a drift in the integral value. This accumulation of errors is not observed in the conservation of the primary variables density, momentum and total energy (not shown here). On the other hand, the global value of kinetic energy presents clear oscillations for EC^B and EC^F schemes, which is likely connected to the first order discretization of the pressure term that governs the exchange between kinetic and internal

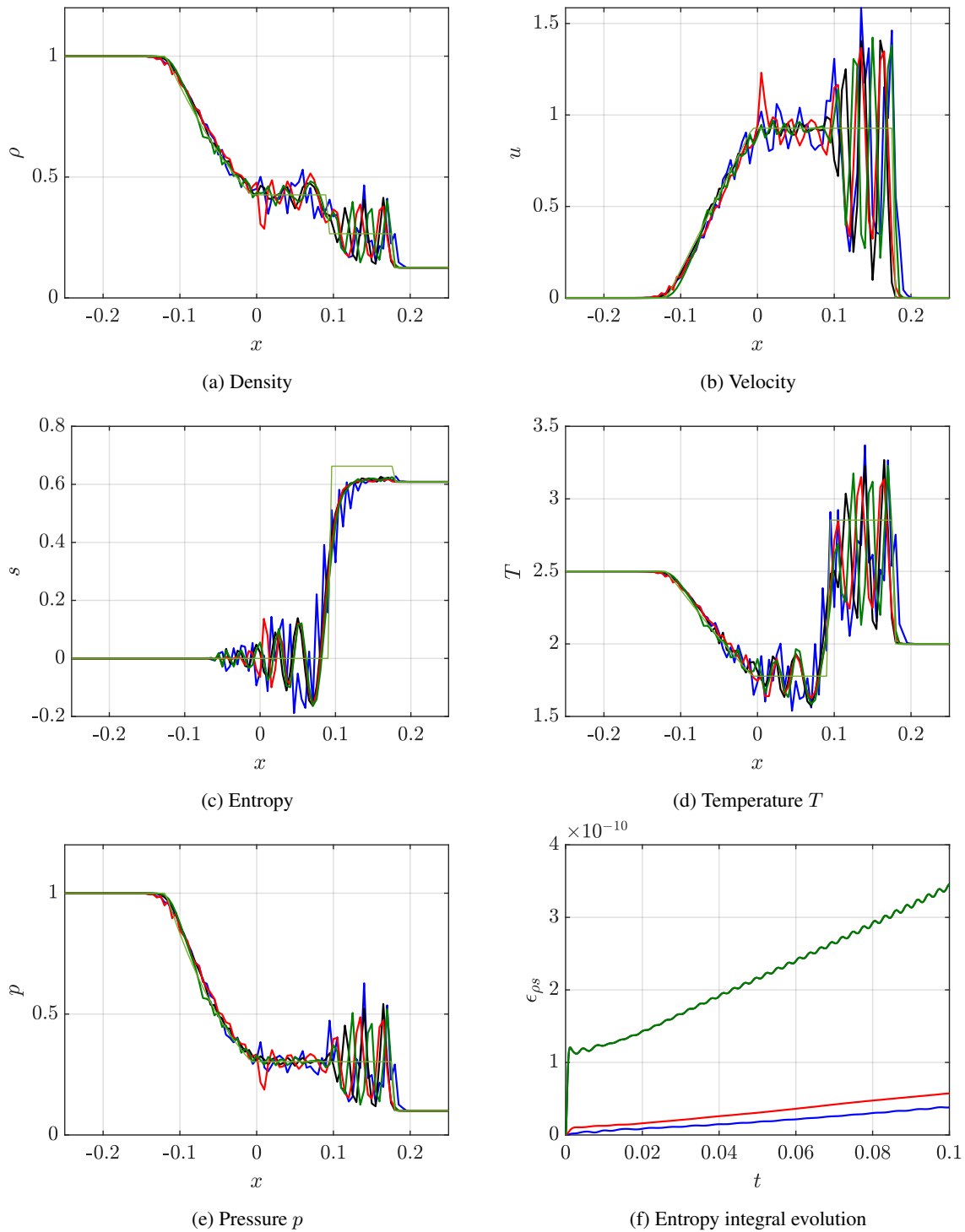


Figure 3: Sod test for different discretizations: black lines are used for EC^B , red for EC^S , green for EC^F , blue EC^W ; pale green line is the exact solution. CFL = 0.01, final solutions at $T = 0.1$.

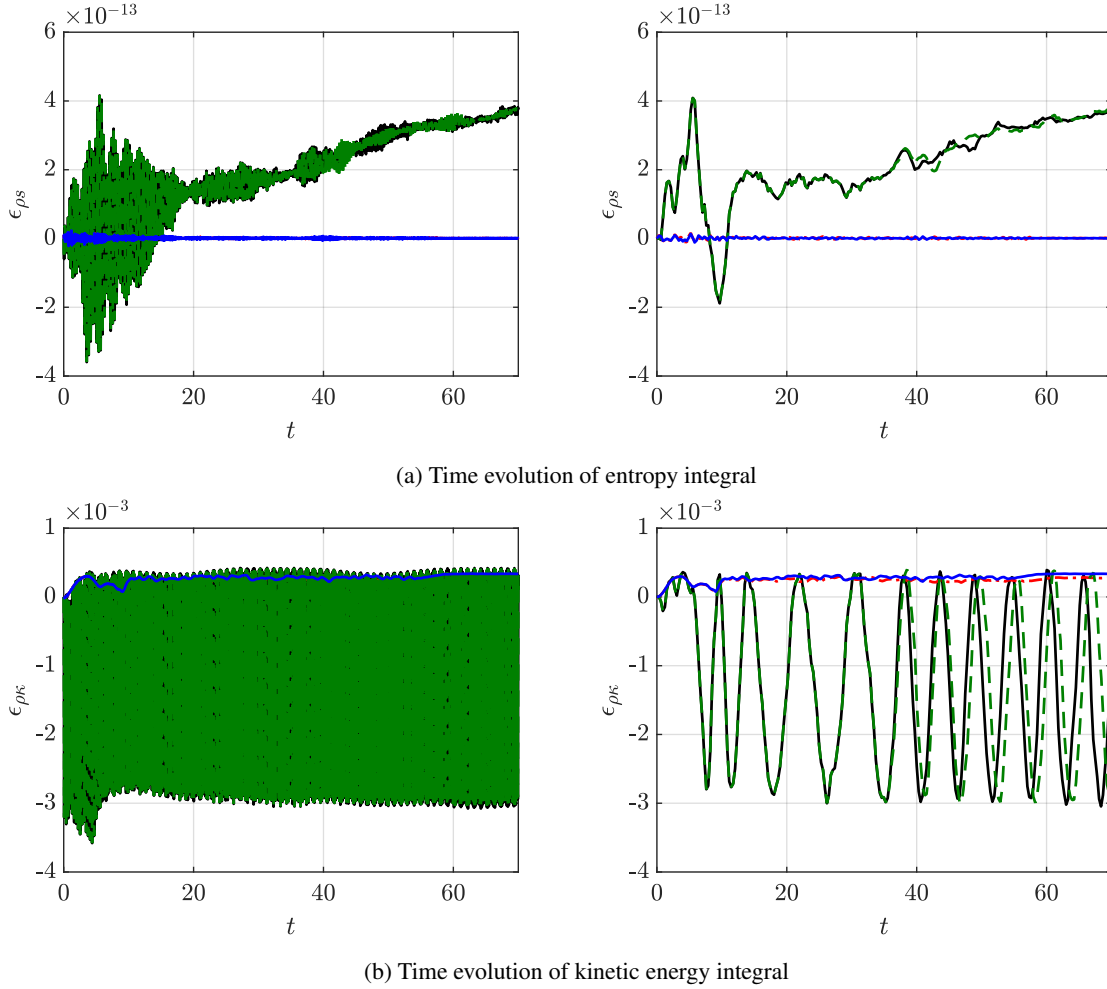


Figure 4: Taylor-Green vortex test for different discretizations: black lines are used for EC^B , red for EC^S , green for EC^F , blue EC^W . On the left-hand side, global quantities are evaluated at each time step of the simulation; on the right-hand side, they are sampled every 200 steps. CFL = 0.01.

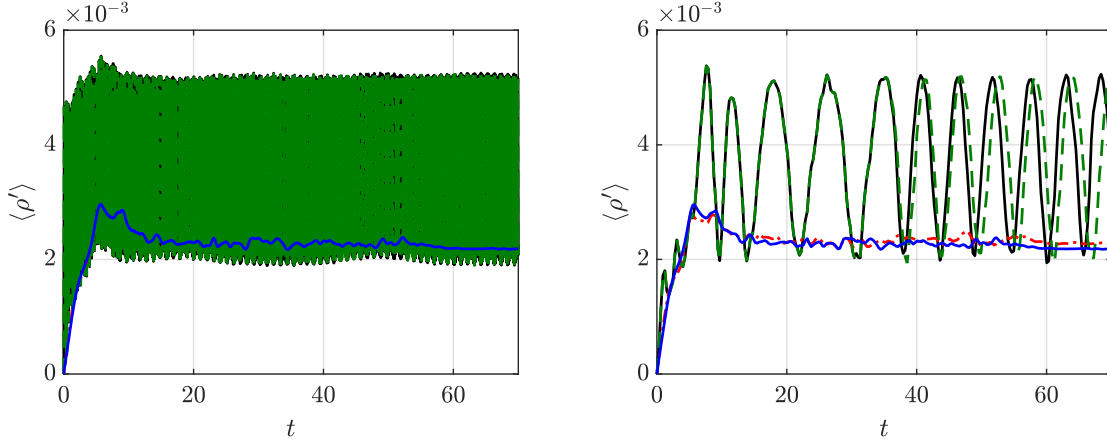
energy. Fig. 4b shows the evolution of global kinetic energy considering the value at each time step of the simulation (on the left) and, for additional clarity, sampling every 200 steps (on the right)⁸.

A similar behavior is also displayed for the evolution of density and temperature fluctuation ρ' and T' in Fig. 5. However, despite the oscillations, none of the schemes yield an unbounded growth of the thermodynamic fluctuations. This is a desirable outcome since, after an initial transient, the flow should behave like inviscid isotropic homogeneous turbulence [20, 21, 56]. This successful result should not to be taken for granted, as many discretizations fail this test and present uncontrolled production in the fluctuations [3, 57].

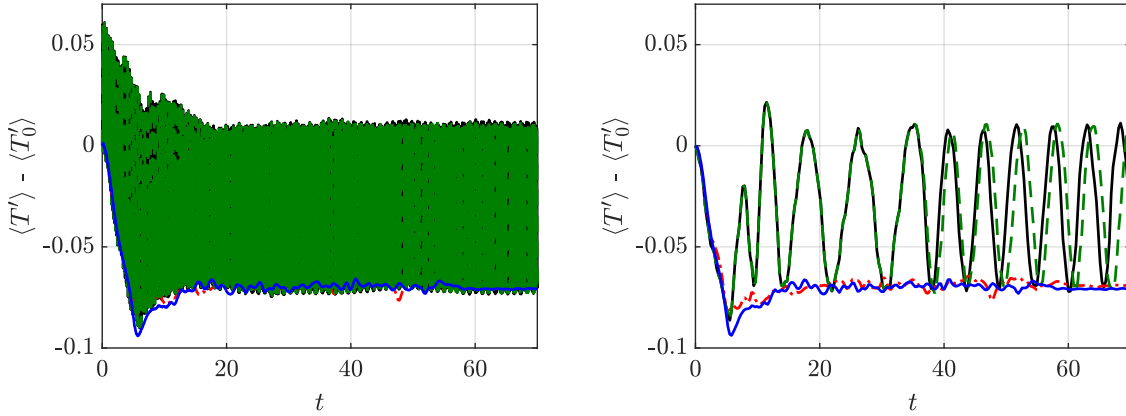
6 Conclusions

The current work introduces a family of entropy conserving schemes for a calorically-perfect single-component gas. The methods have the additional properties of also being kinetic-energy-preserving and pressure-equilibrium-preserving. These schemes are, to the best of our knowledge, the first finite-difference discretizations to be locally conservative in both the primary quantities (mass, momentum, total energy) as well as the discrete entropy dynamics. Their ability to attain exact discrete conservation is confirmed with a variety of test cases in one-, two- and three-dimensions; meanwhile, the propagation of a density wave is also simulated to test the PEP property of the schemes.

⁸The under-sampled plots suggest a leading behavior for the EC^F scheme after awhile; however, this is an artifact of the chosen sampling rate.



(a) Time evolution of density fluctuations



(b) Time evolution of temperature fluctuations

Figure 5: Taylor-Green vortex test for different discretizations: black lines are used for EC^B, red for EC^S, green for EC^F, blue EC^W. On the left-hand side, fluctuations are evaluated at each time step of the simulation; on the right-hand side, they are sampled every 200 steps. CFL = 0.01.

The new framework introduces and leverages FD representations of the logarithmic mean, which is commonly employed in EC numerical fluxes. This equivalence is just one instance of a more general link between linear and nonlinear two-point interpolants and FD forms involving the ratio of differentials. Some of the most commonly used means (e.g., arithmetic, geometric, harmonic) are also provided in this paper. While the schemes presented in this work are initially introduced in the context of finite differencing, they are also locally conservative due to their SBP property and therefore admit a local flux form that can be used in a FV or FE setting. Even though we considered uniform grids herein, extension to arbitrary nodal distributions is also possible as long as a diagonal-norm SBP property is available. The corresponding EC property of the methods is based on point-wise cancellations of spurious volumetric terms that would otherwise be induced in the discrete entropy equation. The proposed FD methods furthermore are expected to work on general triangle/tetrahedral grids via a recent extension of the SBP framework to tensor-product spectral-element operators on collapsed coordinates [58]. In addition, while the current results consider single-block periodic domains, incorporating entropy-stable interface conditions for boundaries and inter-block coupling is possible via Simultaneous Approximation Terms [33, 59], as is typically done with SBP-compatible nonlinear flux methods.

Different avenues for future development remain. First, the schemes presented in this paper admit the possibility of using non-symmetric EC fluxes; such biased forms could be useful in the context of reducing oscillations around sharp gradient fields, and exploring this topic could be the subject of future research. Secondly, the methods' extension to high-order stems naturally from employing high-order finite difference stencils to the differential definitions of the specialized averages; however, this will require extending the two-point algorithm for logarithmic means [47] to a multi-point format that is capable of effectively treating instances where the quotient formula becomes singular. In

the meantime, however, Appendix A provides an alternate error-reducing treatment based on flux differencing for the narrow-width biased methods. Finally, the prospect of extending the current framework to general equations of state per the recent work of Aiello et al. [60] is to be explored.

A Reducing errors in the biased EC schemes via flux differencing

The current FD-EC methods would naturally extend to high-order upon employing high-order derivative formulas within the differencing as well as the FD definitions of the specialize averages. However, the latter requires the development of new multi-point algorithms for calculating the mean quantities while appropriately handling the risk of a singularity when evaluating the quotient expressions. Here, in the meantime, we propose a error-reducing extension of the narrow biased FD-EC schemes based on flux differencing.

Per Remark 2, the FD-EC methods imply satisfaction of a local entropy conserving flux condition. High-order flux reconstructions are then typically viable via combinations of symmetric two-point fluxes [41]. The two-point functions of the biased schemes, however, are no longer symmetric in their arguments (i.e., the order in which the solution vectors q are supplied informs the respective biases of the velocity and the pressure); therefore, this nuance needs to be accounted for within the flux differencing definition as

$$\frac{\mathcal{F}_{i+1/2}^{(n)} - \mathcal{F}_{i-1/2}^{(n)}}{h_i \cdot \Delta x} = \frac{1}{\Delta x} \left(\sum_{k \leq 0} 2d_{i,i+k}^c \cdot \mathcal{F}^{(n)}|_{2\text{pt}}^\alpha(q_{i+k}, q_i) + \sum_{k > 0} 2d_{i,i+k}^c \cdot \mathcal{F}^{(n)}|_{2\text{pt}}^\alpha(q_i, q_{i+k}) \right) \quad (46)$$

where

$$\mathcal{F}^{(n)}|_{2\text{pt}}^\alpha(q_a, q_b) = \begin{bmatrix} \mathcal{F}_\rho^{(n)}|_{2\text{pt}}^\alpha \\ \mathcal{F}_{\rho u_m}^{(n)}|_{2\text{pt}}^\alpha \\ \mathcal{F}_{\rho E}^{(n)}|_{2\text{pt}}^\alpha \end{bmatrix} = \begin{bmatrix} \overline{(\rho_a, \rho_b)}^{\log, n} ((1 - \alpha) \cdot u_{n,a} + \alpha \cdot u_{n,b}) \\ \mathcal{F}_\rho^{(n)}|_{2\text{pt}}^\alpha \cdot \frac{(u_{m,b} + u_{m,a})}{2} + \delta_{mn} \cdot ((1 - \alpha) \cdot p_b + \alpha \cdot p_a) \\ \mathcal{F}_\rho^{(n)}|_{2\text{pt}}^\alpha \cdot \left(\sum_{m=1}^d \frac{u_{m,a} u_{m,b}}{2} + \overline{(e_a, e_b)}^{H \log, n} \right) + (1 - \alpha) \cdot u_{n,a} p_b + \alpha \cdot u_{n,b} p_a \end{bmatrix}. \quad (47)$$

In the above, $d_{i,i+k}^c$ are the stencil coefficients associated with a *central* SBP operator evaluated at node i . While the fluxes are fully biased with respect to the advective velocity and the pressure, these quantities are *counter-balanced* and therefore the overall method and its fluxes can be interpreted as being ‘‘centered’’. As such, a central SBP operator in the prescription of the $d_{i,i+k}^c$ coefficients is still appropriate. The multi-point flux associated with the above is (see Eq. 3.9 in [41])

$$\mathcal{F}^{(n)}|_{\text{multi-pt}}^\alpha = \sum_{k > 0} \sum_{\ell \leq 0} 2d_{i+\ell, i+k}^c \cdot \mathcal{F}^{(n)}|_{2\text{pt}}^\alpha(q_{i+\ell}, q_{i+k}). \quad (48)$$

The strict biasing of the velocity and pressure that results from the asymmetric flux function can be expected to limit the above to first order. Namely, despite the $d_{i,i+k}$ coefficients stemming from a high-order central operator, they do not allow for the necessary error cancellations within the velocity and pressure variables, which are fully biased. Even though formal asymptotic accuracy is not increased, employing such stencils can be made to reduce errors in the solutions.

Here we revisit the isentropic vortex and Sod shock tube test cases from Section 5 in order to survey the newly proposed methods; we focus on the backward biased EC^B and symmetric EC^S renditions for brevity. The long-time entropy conservation of the new formulations are confirmed (see Figures 6b and 7f). Meanwhile, the convergence test on the isentropic vortex (see Figure 6a) shows that the current multi-point flux-differencing of the biased schemes are still limited to first order; however, the error constant is reduced from the nominal two-point second order method previously shown in Figure 1a. Despite not being formally high-order, the current multi-point flux-differencing extension of the biased schemes is also seen to reduce oscillations in Sod shock tube results compared to the symmetric flux (see Figure 7). This property therefore motivates the potential utility of such schemes for flows exhibiting sharp gradients.

Acknowledgments

CDM and GC acknowledge the CINECA award under the ISCRA initiative, for the availability of high-performance computing resources and support. The second author (AE) acknowledges funding for this work from the Air Force Office of Scientific Research (AFOSR) (program officers: Drs. Chiping Li and Fariba Farhoo) under contract No. 22RQCOR003, as well as Jacobs Engineering Inc. under contract No. FA9300-20-F-9801.

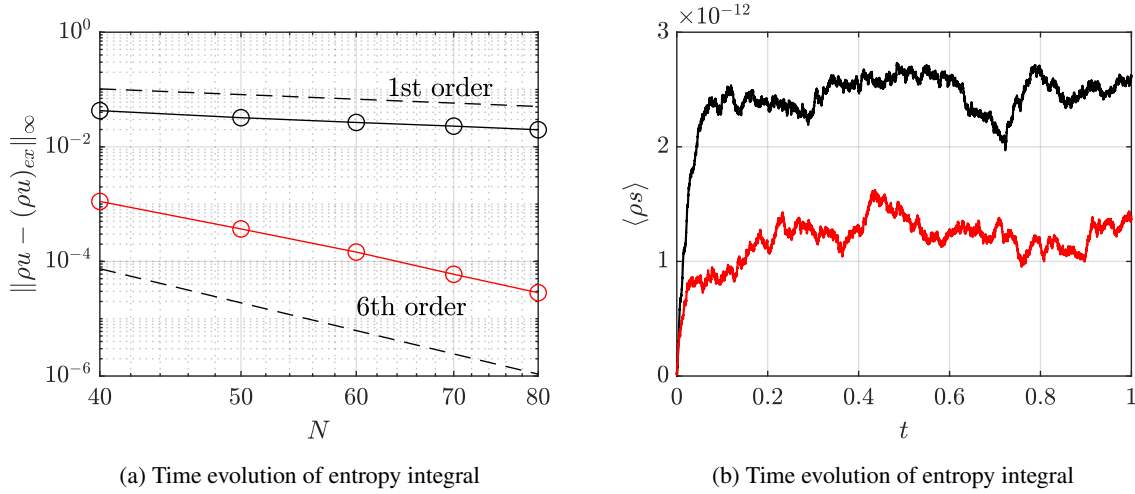


Figure 6: Isentropic vortex test for different discretizations using flux differencing: solid black lines are used for EC^B and red for EC^S . $CFL = 0.01$.

References

- [1] A. E. P. Veldman, Supraconservative finite-volume methods for the Euler equations of subsonic compressible flow, *SIAM Rev.* 63 (2021) 756–779.
- [2] W. Rozema, J. C. Kok, R. W. C. P. Verstappen, A. E. P. Veldman, A symmetry-preserving discretisation and regularisation model for compressible flow with application to turbulent channel flow, *J. Turbul.* 34 (2014) 386–410.
- [3] Y. Kuya, K. Totani, S. Kawai, Kinetic energy and entropy preserving schemes for compressible flows by split convective forms, *J. Comput. Phys.* 375 (2018) 823–853.
- [4] N. Shima, Y. Kuya, Y. Tamaki, S. Kawai, Preventing spurious pressure oscillations in split convective form discretization for compressible flows, *J. Comput. Phys.* 427 (2021) 110060.
- [5] R. Abgrall, F. N. Mojarrad, Conservative scheme compatible with some other conservation laws: conservation of the local angular momentum, *Comput. Fluids* 247 (2022).
- [6] A. K. Edoh, A new kinetic-energy-preserving method based on the convective rotational form, *J. Comput. Phys.* 454 (2022) 110971.
- [7] A. Gouasmi, K. Duraisamy, S. M. Murmann, Formulation of entropy-stable schemes for the multicomponent compressible Euler equations, *Comput. Methods Appl. Mech. Eng.* 363 (2020).
- [8] A. Peyvan, K. Shukla, J. Chan, G. E. Karniadakis, High-order methods for hypersonic flows with strong shocks and real chemistry, *J. Comput. Phys.* 490 (2023).
- [9] E. J. Ching, R. F. Johnson, A. D. Kercher, Positivity-preserving and entropy-bounded discontinuous Galerkin method for chemically reacting, compressible Euler equations. Part I: The one-dimensional case, *J. Comput. Phys.* (2024).
- [10] A. Arakawa, Computational design for long-term numerical integration of the equations of fluid motion: Two-dimensional incompressible flow. Part I, *J. Comput. Phys.* 1 (1966) 119–143.
- [11] Y. Morinishi, T. S. Lund, O. V. Vasilyev, P. Moin, Fully conservative higher order finite difference schemes for incompressible flows, *J. Comput. Phys.* 143 (1998) 90–124.
- [12] P. S. Volpiani, A comprehensive study about implicit/explicit large-eddy simulations with implicit/explicit filtering, *Flow Turbul. Combust.* (2024).
- [13] A. Harten, On the symmetric form of system of conservation laws with entropy, *J. Comput. Phys.* 49 (1983) 151–164.
- [14] M. L. Merriam, An Entropy-based Approach to Nonlinear Stability, Technical Report, NASA Ames Research Center, 1989.
- [15] E. Tadmor, The numerical viscosity of entropy stable schemes for systems of conservation laws. I, *Math. Comput.* 179 (1987) 91–103.

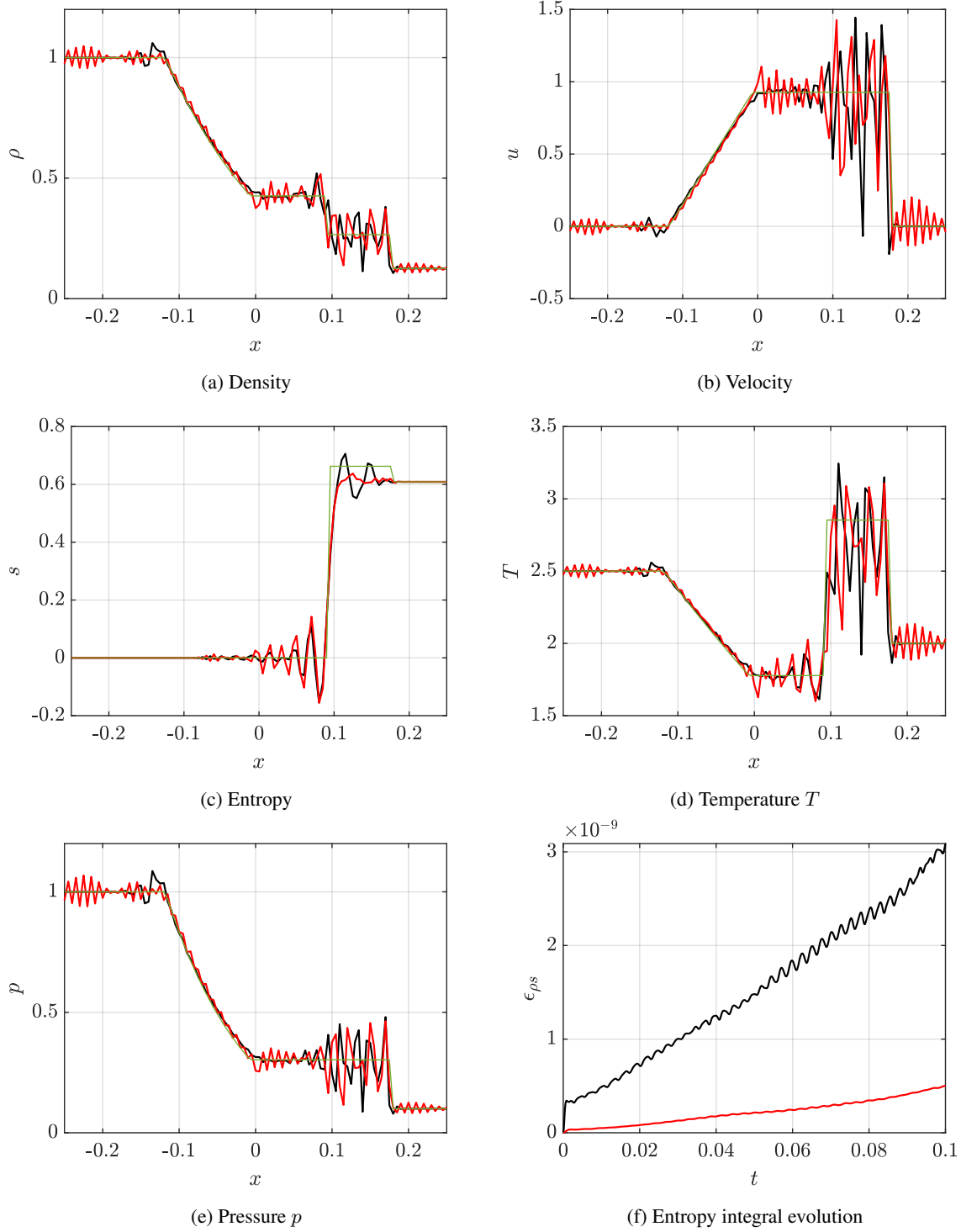


Figure 7: Sod test for different discretizations using flux differencing: black lines are used for EC^B and red for EC^S; pale green line is the exact solution. Final solutions at $T = 0.1$ based on CFL = 0.01.

- [16] P. G. LeFloch, J. M. Mercier, C. Rhode, Fully discrete, entropy conservative schemes of arbitrary order, *SIAM J. Numer. Anal.* 40 (2002) 1968–1992.
- [17] T. Fisher, M. Carpenter, N. J., N. Yamaleev, C. Swanson, Discretely conservative finite-difference formulations for nonlinear conservation laws in split form: Theory and boundary conditions, *J. Comput. Phys.* 234 (2013) 353–375.
- [18] G. J. Gassner, A skew-symmetric discontinuous Galerkin spectral element discretization and its relation to SBP-SAT finite difference methods, *SIAM J. Sci. Comput.* 35 (2013) A1233–A1253.
- [19] H. Ranocha, M. Schlottke-Lakemper, J. Chan, A. R. W. A. M. Rueda-Ramirez, F. Hindenlang, G. Gassner, Efficient implementation of modern entropy stable and kinetic energy preserving discontinuous Galerkin methods for conservation laws, *ACM Trans. Math. Soft.* 49 (2023) 1–30.
- [20] S. Pirozzoli, Generalized conservative approximations of split convective derivative operators, *J. Comput. Phys.* 229 (2010) 7180–7190.
- [21] G. Coppola, F. Capuano, S. Pirozzoli, L. de Luca, Numerically stable formulations of convective terms for turbulent compressible flows, *J. Comput. Phys.* 382 (2019) 86–104.
- [22] R. D. Richtmeyer, K. W. Morton, *Difference Methods for Initial Value Problems*, Interscience, 1967.
- [23] A. Jameson, The construction of discretely conservative finite volume schemes that also globally conserve energy or entropy, *J. Sci. Comput.* 34 (2008) 152–187.
- [24] Y. Tamaki, Y. Kuya, S. Kawai, Comprehensive analysis of entropy conservation property of non-dissipative schemes for compressible flows: KEEP scheme redefined, *J. Comput. Phys.* 468 (2022) 111494.
- [25] H. Ranocha, Generalised Summation-by-Parts Operators and Entropy Stability of Numerical Methods for Hyperbolic Balance Laws, Ph.D. thesis, der Technischen Universität Carolo-Wilhelmina zu Braunschweig, 2018.
- [26] H. Ranocha, G. J. Gassner, Preventing pressure oscillations does not fix local linear stability issues of entropy-based split-form high-order schemes, *Commun. Appl. Math. Comput.* 4 (2022) 880–903.
- [27] P. Chandrashekar, Kinetic energy preserving and entropy stable finite volume schemes for compressible Euler and Navier-Stokes equations, *Commun. Comput. Phys.* 14 (2013) 1252–1286.
- [28] C. De Michele, G. Coppola, Asymptotically entropy-conservative and kinetic-energy preserving numerical fluxes for compressible Euler equations, *J. Comput. Phys.* 492 (2023) 112439.
- [29] G. A. Blaisdell, E. T. Spyropoulos, J. H. Qin, The effect of the formulation of nonlinear terms on aliasing errors in spectral methods, *Appl. Numer. Math.* 21 (1996) 207–219.
- [30] C. A. Kennedy, A. Gruber, Reduced aliasing formulations of the convective terms within the Navier-Stokes equations for a compressible fluid, *J. Comput. Phys.* 227 (2008) 1676–1700.
- [31] A. K. Edoh, Conservative correction procedures utilizing artificial dissipation operators, *J. Comput. Phys.* 504 (2024) 112880.
- [32] D. C. Del Rey Fernandez, P. D. Boom, D. W. Zingg, A generalized framework for nodal first derivative summation-by-parts operators, *J. Comput. Phys.* 266 (2014) 214–239.
- [33] D. C. Del Rey Fernandez, J. E. Hicken, D. W. Zingg, Review of summation-by-parts operators with simultaneous approximation terms for the numerical solution of partial differential equation, *Comput. Fluids* 95 (2014) 171–196.
- [34] K. Mattsson, Diagonal-norm upwind SBP operators, *J. Comput. Phys.* 355 (2017) 283–310.
- [35] H. Ranocha, A. R. Winters, M. Schlottke-Lakemper, P. Offner, J. Glaubitz, G. J. Gassner, On the robustness of high-order upwind summation-by-parts methods for nonlinear conservation laws, *J. Comput. Phys.* (2024).
- [36] C. Williams, K. Duru, Full-spectrum dispersion relation preserving summation-by-parts operators, *SIAM J. Numer. Anal.* 62 (2024).
- [37] G. Coppola, A. E. P. Veldman, Global and local conservation of mass, momentum and kinetic energy in the simulation of compressible flow, *J. Comput. Phys.* 475 (2023) 111879.
- [38] L. Dovgilevich, I. Sofronov, High-accuracy finite-difference schemes for solving elastodynamic problems in curvilinear coordinates within multiblock approach, *Appl. Numer. Math.* 93 (2015) 176–194.
- [39] J. E. Hicken, D. W. Zingg, Summation-by-parts operators and high-order quadrature, *J. Computat. Appl. Math.* 237 (2013) 111–125.
- [40] T. C. Fisher, M. H. Carpenter, J. Nordstrom, N. K. Yamaleev, Discretely conservative finite-difference formulations for nonlinear conservation laws in split form: Theory and boundary conditions, *J. Comput. Phys.* 234 (2013) 353–375.

- [41] T. C. Fisher, M. H. Carpenter, High-order entropy stable finite difference schemes for nonlinear conservation laws: Finite domains, *J. Comput. Phys.* 252 (2013) 518–557.
- [42] A. G. Kravchenko, P. Moin, On the effect of numerical errors in large eddy simulations of turbulent flows, *J. Comput. Phys.* 131 (1997) 310–322.
- [43] A. K. Edoh, N. L. Mundis, A. R. Karagozian, V. Sankaran, Balancing aspects of numerical dissipation, dispersion, and aliasing in time-accurate simulations, *Int. J. Numer. Methods Fluids* 92 (2020) 1506–1527.
- [44] Y. Kuya, S. Kawai, Modified wavenumber and aliasing errors of split convective forms for compressible flows, *J. Comput. Phys.* 464 (2022).
- [45] J. Reiss, J. Sesterhenn, A conservative, skew-symmetric finite difference scheme for the compressible Navier-Stokes equations, *Comput. Fluids* 101 (2014) 208–219.
- [46] H. Chen, Means generated by an integral, *Math. Mag.* 78 (2005) 397–399.
- [47] F. Ismail, P. L. Roe, Affordable, entropy-consistent Euler flux functions II: Entropy production at shocks, *J. Comput. Phys.* 228 (2009) 5410–5436.
- [48] K. B. Stolarsky, Generalizations of the logarithmic mean, *Math. Mag.*, 48 (1975) 87–92.
- [49] K. B. Stolarsky, The power and generalized logarithmic means, *Am. Math. Mon.* 87 (1980) 545–548.
- [50] W. J. Feiereisen, W. C. Reynolds, J. H. Ferziger, Numerical Simulation of Compressible, Homogeneous Turbulent Shear Flow, Technical Report TF-13, Stanford University, 1981.
- [51] H. Ranocha, Comparison of some entropy conservative numerical fluxes for the Euler equations, *J. Sci. Comput.* 76 (2018) 216–242.
- [52] A. R. Winters, C. Czernik, M. B. Schily, G. J. Gassner, Entropy stable numerical approximations for the isothermal and polytropic Euler equations, *BIT Numer. Math.* 60 (2020) 791 – 824.
- [53] C. De Michele, G. Coppola, Novel pressure-equilibrium and kinetic-energy preserving fluxes for compressible flows based on the harmonic mean, *J. Comput. Phys.* 518 (2024) 113338.
- [54] Y. Fujiwara, Y. Tamaki, S. Kawai, Fully conservative and pressure-equilibrium preserving scheme for compressible multi-component flows, *J. Comput. Phys.* 478 (2023) 111973.
- [55] M. Bernardini, D. Modesti, F. Salvatore, S. Sathyanarayana, G. Della Posta, S. Pirozzoli, STREAMS-2.0: Supersonic turbulent accelerated Navier-Stokes solver version 2.0, *Comput. Phys. Commun.* 285 (2023) 108644.
- [56] A. E. Honein, P. Moin, Higher entropy conservation and numerical stability of compressible turbulence simulations, *J. Comput. Phys.* 201 (2004) 531 – 545.
- [57] C. De Michele, G. Coppola, Numerical treatment of the energy equation in compressible flows simulations, *Comput. Fluids* 250 (2023) 105709.
- [58] T. Montoya, D. W. Zingg, Efficient entropy-stable discontinuous spectral-element methods using tensor-product summation-by-parts operators on triangles and tetrahedra, *J. Comput. Phys.* (2024).
- [59] M. Svard, Entropy stable boundary conditions for the Euler equations, *J. Comput. Phys.* 426 (2021).
- [60] A. Aiello, C. De Michele, G. Coppola, Entropy conservative discretization of compressible Euler equations with an arbitrary equation of state, <https://arxiv.org/pdf/2408.01235v1> (2024).